High-Performance Nanostructured Palladium-Based Hydrogen Sensors - Current Limitations and Strategies for Their Mitigation

ACS SENSORS

pubs.acs.org/acssensors

Perspective

High-Performance Nanostructured Palladium-Based Hydrogen Sensors—Current Limitations and Strategies for Their Mitigation

Iwan Darmadi,* Ferry Anggoro Ardy Nugroho,* and Christoph Langhammer*

Cite This: *ACS Sens.* 2020, 5, 3306−3327

Read Online

ACCESS | Metrics & More | Article Recommendations

ABSTRACT: Hydrogen gas is rapidly approaching a global breakthrough as a carbon-free energy vector. In such a hydrogen economy, safety sensors for hydrogen leak detection will be an indispensable element along the entire value chain, from the site of hydrogen production to the point of consumption, due to the high flammability of hydrogen−air mixtures. To stimulate and guide the development of such sensors, industrial and governmental stakeholders have defined sets of strict performance targets, which are yet to be entirely fulfilled. In this Perspective, we summarize recent efforts and discuss research strategies for the development of hydrogen sensors that aim at meeting the set performance goals. In the first part, we describe the state-of-the-art for fast and selective hydrogen sensors at the research level, and we identify nanostructured Pd transducer materials as the common denominator in the best performing solutions. As a consequence, in the second part, we introduce the fundamentals of the Pd−hydrogen interaction to lay the foundation for a detailed discussion of key strategies and Pd-based material design rules necessary for the development of next generation high-performance nanostructured Pd-based hydrogen sensors that are on par with even the most stringent and challenging performance targets.

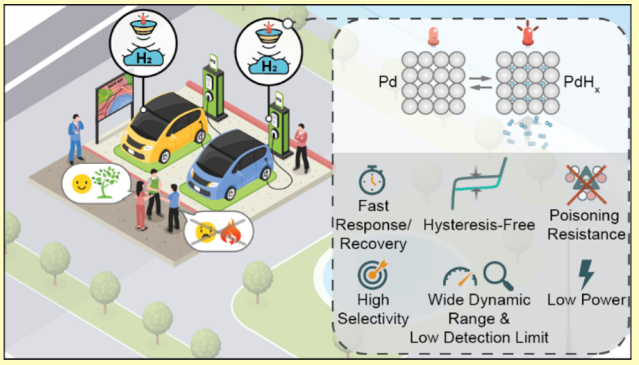

KEYWORDS: *palladium, alloy, nanostructure, nanomaterial, nanoparticle, state-of-the-art, performance target, design rules*

To achieve the necessary dramatic reduction of greenhouse gas emissions, alternative energy vectors that replace fossil fuels are imperative. In this respect, hydrogen gas, H_2, has been identified as particularly attractive since it can be used to generate electricity with water as the only byproduct.[1] Therefore, large investments in a hydrogen economy are imminent all over the globe, as, for example, in Europe, as part of the Green Deal.[2,3] Until very recently, one specific technological challenge related to a widespread use and large-scale distribution of hydrogen gas had received little attention in the public debate, but came to broad attention due to a recent accident at a Norwegian H_2 fuel station[4]—hydrogen safety. This event was a dramatic reminder of the high flammability of H_2−air mixtures at H_2 concentrations above 4%, and thus made the importance of robust and fast hydrogen safety sensors for leak detection highly apparent. However, to date, no hydrogen sensor technology exists that can meet all the hydrogen safety sensor performance targets set by, for example, the US Department of Energy (DoE),[5] despite at least a decade of research (Scheme 1).[6−15]

In this Perspective, we therefore first critically assess the current state-of-the-art of high-performance hydrogen sensors across all signal transducer platforms. With high performance, here we mean sensors that have been developed with the aim and/or potential to meet the US DoE hydrogen sensor performance targets. This approach thus sets apart our focus of discussion from other more conventional review articles on the topic.[10−16] In the second part of this work, based on the literature survey, we conclude and propose that nanostructured materials based on palladium (Pd) and its alloys are the signal transducer materials known today with the best potential to eventually meet all of the US DoE performance targets for hydrogen safety sensors. To reach this conclusion, we thoroughly discuss the fundamentals of Pd−H interactions to identify the fundamental material properties that intrinsically limit sensor performance. Based on this understanding, we then derive rational material design rules and summarize a selection of existing research efforts that already utilize some of those rules. Last, we propose and discuss future research directions, mainly focusing on the likely most challenging US DoE targets: (i) sensor lifetime, (ii) operation temperature, (iii) absolute operation pressure, (iv) operation in poisoning/deactivating

Received: September 28, 2020
Accepted: October 27, 2020
Published: November 12, 2020

https://dx.doi.org/10.1021/acssensors.0c02019
ACS Sens. 2020, 5, 3306−3327

Scheme 1. US DoE Performance Targets for Stationary and Automotive Hydrogen Safety Sensors[5]

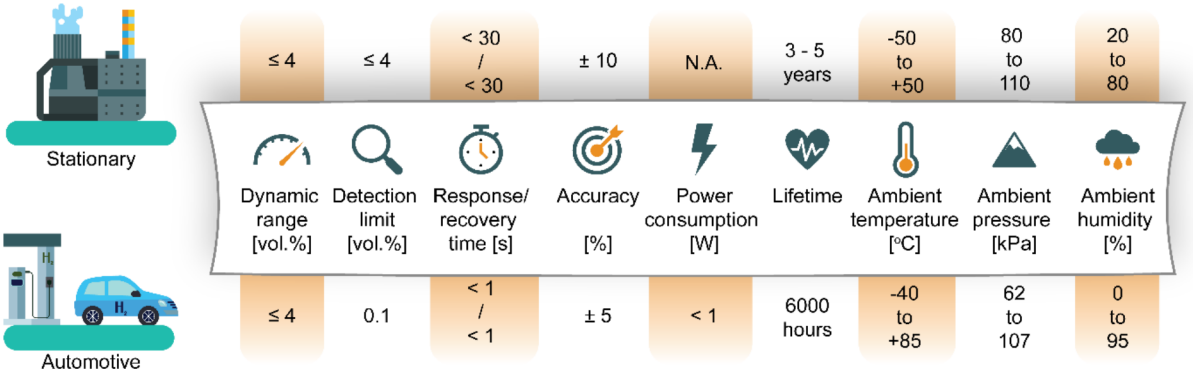

conditions, and (v) at high humidity, in order to hopefully inspire rapid development efforts in these directions.

HYDROGEN SENSOR STATE-OF-THE-ART WITH RESPECT TO THE US DOE TARGETS

Response Time. The sensor response time target probably constitutes one of the most challenging targets to meet, but also one of the most obvious ones to rationalize why it is important from a safety perspective.[17] Thus, response time has been a key topic in many studies, and we have found 553 relevant reports from 1999 to 2020 that claim "fast hydrogen sensors".[18] In terms of operating conditions, they range from room temperature (RT) up to 500 °C. The highest temperatures are predominantly reported for oxide-based sensors, where they are needed to enable efficient ionic transport. This wide range of operation temperatures, however, makes direct comparison of different types of sensors somewhat difficult since, at least for the same type of active material, higher operating temperatures will lead to faster response times, as a consequence of the Arrhenius law. Therefore, to allow relevant comparison, and to keep our focus on high-performance sensors that operate at the toughest conditions, we have opted to only include sensors that operate at (or close to) RT in our survey. In this way, we are also directly addressing the power consumption target, which intrinsically is harder to meet for a sensor that needs to be maintained at high operating temperature. Furthermore, to enable direct comparison between different sensors, we use t_{90}, that is, the time to reach 90% of the sensor response for the new steady state after a stimulus, as descriptor for response time. Finally, wherever possible, we have used the response corresponding to a hydrogen exposure to 0.1 vol.% (~1000 ppm ≈ 1 mbar), i.e., the lower hydrogen detection limit in the US DoE performance target. This is important not only from the perspective of identifying this number as the ultimate goal, but also since many experiments[19−23] suggest that the response time depends on both the absolute hydrogen concentration and the amplitude of pressure change to be detected. In other words, a hydrogen sensor generally will respond faster when exposed to a larger concentration change. Hence, this fact has to be taken into consideration when comparing the speed of different sensors, and thus we only list sensors measured at hydrogen concentrations equal to or less than 0.1 vol.% and those reporting maximum 5 s response time when exposed to a H_2 concentration higher than 0.1 vol.%. As summarized in Table 1, only around 10% of the surveyed works (i.e., 58 out of 553) when using the search string introduced above fall into our category, and we make the following observations.

The first key point to note is that in terms of readout principle, electrical sensors (resistance-based), which comprise two electrodes connected to a transducer element that changes resistivity upon interaction with hydrogen, are most abundant among the systems with fast response according to our definition. The typical transducer materials for this resistive-based electrical sensors are Pd, metal oxides (e.g., SnO_2, TiO_2, In_2O_3, ZnO, MoO_3, and WO_3) or a hybrid of Pd and a metal oxide. This is no surprise, since this type of sensor is most mature and has a simple, yet effective, construction. Interestingly, however, from a commercial hydrogen sensor market perspective, they are not the most common ones available.[81] The second key observation is that in terms of active material, the majority of fast sensors employ Pd and its alloys in various forms. The third and maybe most striking finding is that *all* fast hydrogen sensors employ some sort of nanostructured transducer element(s). This development has been enabled by the parallel advances in nanoparticle synthesis and nanofabrication, and it was triggered by Favier et al.'s seminal work on ultrafast Pd nanowire array electrical hydrogen sensors from 2001,[40] the first sensor to achieve millisecond response time to 5 vol % H_2 (Figure 1a).

However, if we take the US DoE's most stringent response time target (<1 s at 0.1 vol % H_2), even to date, still only a few works *may* have or *do* have reached this target at RT. For example, Lee et al.'s porous Pd@CPPy conducting polymer[24] and Zhang et al.'s SnO_2@graphene[27] hydrogen sensors *may* have reached the 1 s target (Figure 1b). Specifically, Lee et al. and Zhang et al. recorded 4.5 and 2 s response times, respectively, at extremely low H_2 concentrations of 20 ppm (~0.002 vol %) and 100 ppm (~0.01 vol %) in air. Thus, as discussed above, if measured at a higher concentration of 0.1 vol %, these sensors *may*, in principle, respond faster than the 4.5 and 2 s reported at those low ppm and thus meet the US DoE target. However, no explicit measurement is presented by the authors. Similarly, there are some works that report response times close to the 1 s at the 0.1 vol % limit. For example, porous PdPt thin film (5 s at 1000 ppm),[44] Pd ultrathin films (0.07 s at 2 vol %),[34] and Pd nanowire arrays (0.075 s at 5 vol %).[40] Thus, to the best of our knowledge, Nugroho et al.'s recent work using PdAu alloy nanoparticle@polymer nanocomposite materials and Chen et al. Pt@SnO_2 nanowires are the only work that *explicitly* demonstrates a response time of ~1 s at 1 mbar and 1000 ppm H_2, respectively (Figure 1c).[19,29] However, we also note that in Nugroho et al.'s work the response was obtained in an idealized pure H_2/vacuum environment. As we discuss in the next chapter, this is a significant limitation since interference and

https://dx.doi.org/10.1021/acssensors.0c02019
ACS Sens. 2020, 5, 3306−3327

Table 1. Fast Hydrogen Sensors in the Literature[18] Operated at Room Temperature

active materials[a]	transducer platform	response time, t_{90} (s)	recovery time, t_{10} (s)	measured at pressure	background environment	LoD[b] (ppm)	ref
Pd NP@CPPy	Electrical	4.5	27	20 ppm	Air	0.1	24
Pd/Au thin film on pSiC	Electrical	2.3	1.5	40 ppm	Air	10	25
Pd@Al_2O_3/TiO_2	Electrical	30	-	5 ppm	N_2	-	26
SnO_2 NP@graphene	Electrical	2	4	100 ppm	Air	1	27
MoO_3 NR	Electrical	3	16	100 ppm	Air	-	28
Pt@SnO_2 NR	Electrical	0.3	87	1000 ppm	Air	-	29
PdAu NP @PTFE/PMMA	Optical	1	5	1 mbar	Vacuum	1	19
Sericin protein@ZnO NR	Electrical	11	7	100 ppm	Air	10	30
Pd-coated rare earth thin film	Electrical	0.44	-	0.25 vol %	Air	156	31
Ru@CPPy	Electrical	12	32	100 ppm	N_2	0.5	32
Pd/ZnO NW	Electrical	13	17	100 ppm	Air	0.02	33
Pd ultrathin film	Electrical	0.068	-	2 vol %	N_2	25	34
Thin film metallic glass/diamond/ ZnO NR	Electrical	20	35	100 ppm	Air	-	35
Pd@CNT film	Electrical	7	89	311 ppm	Air	0.89	36
GO nanostructures	Electrical	11	36	200 ppm	-	-	37
Pd thin film	Electrical	60	-	40 ppm	N_2	20	38
$ZnFe_2O_4$−Pd@rGO	Electrical	18	39	200 ppm	N_2	50	39
Pd mesowire	Electrical	0.075	-	5 vol %	N_2	5000	40, 41
Pd NG	Electrical	1	-	0.4 vol %	N_2	-	42
Pt@WO_3 ultrathin film	Electrical	5	20	1000 ppm	Ar	10	43
Porous PdPt thin film	Acoustic	5	-	1000 ppm	N_2	3.7	44
Pd NP/Al_2O_3 NW	Electrical	11	-	0.05 vol %	Ar	500	45
Pd NP@CNT	Electrical	14	-	0.05 vol %	Air	500	46
Pd NW/Al_2O_3	Electrical	0.7	20	1 vol %	Air	-	47
La^{3+}@ZnO NR	Electrical	15	9	500 ppm	Air	5	48
MoO_3 NR/graphene	Electrical	10	30	1000 ppm	Air	0.5	49
Graphite/Pt NP/ZnO	Electrical	10	-	1000 ppm	Air	10	50
Pd NT	Electrical	10	-	0.1 vol %	Ar	-	51
MoO_3 NR	Electrical	11	30	1000 ppm	Air	1	52
Pt@polySi NB	Electrical	11	570	0.1 vol %	N_2	5	53
Pd NW networks	Electrical	11	-	0.1 vol %	N_2	-	54
Pd NP@Si nanomesh	Electrical	12	16	0.1 vol %	Air	-	55
Pd NP on SiO_2	Capacitive	1.2	10	1 vol %	N_2	10000	56
Pd NP	Electrical	5	-	2.5 mbar	Vacuum	100	57
PdAuCu NP	Optical	0.4	5	40 mbar	Vacuum	5	58
Pd NP@ZnO NR	Electrical	18	130	1000 ppm	Air	-	59
TiO_2@PPy	Electrical	20	25	1000 ppm	Air	-	60
PdNi thin film	Acoustical	20	-	0.1 vol %	N_2	-	61
Pd@SnO_2	Electrical	2	-	10000 ppm	Air	40	62
Pd NP@CNT	Electrical	50	400	400 ppm	Air	-	63
Pd thin film	Electrical	3	-	8000 ppm	Air	-	64
Pt NP@WO_3 thin film	Electrical	4.8	3.8	0.5 vol %	N_2	-	65
SnO_2 NP@CNT	Electrical	3	-	1 vol %	Air	-	66
POSS/Pd NP composite	Optical	1	2	3 vol %	Ar	-	67
Porous Pd/TiO_2 film	Electrical	4	10	0.8 vol %	Air	-	68
Pd NP	Electrical	1.5	7.5	2.2 vol %	N_2	100	69
PdCu NW	Acoustical	4	4	1 vol %	Air	7	70
Pd NP on SiO_2 film	Capacitive	1	11	4 vol %	N_2	-	71
Pd NP	Electrical	2	10	2.2 vol %	N_2	100	69
PdNi NP	Electrical	4.5	-	10 mbar	Vacuum	500	72
Pd NG	Electrical	1	-	5 vol %	N_2	200	73
Pt NP on Au microchannels	Electrical	2	184	4 vol %	N_2	1000	74
Pd NS	Electrical	2	5	5 vol %	Ar	-	75
Pd NP@ Si NW	Electrical	2.3	-	5 vol %	N_2	-	76
Pd ultrathin film	Optical	3	10	4 vol %	Ar	-	77
PdCuSi thin film	Capacitive	4.9	-	3 vol %	Air	-	78
Pd@PUA NR	Optical	5.1	-	4 vol %	Air	1000	79
PANI/Sm_2O_3 nanocomposite	Electrical	4	7	8 vol %	Air	-	80

https://dx.doi.org/10.1021/acssensors.0c02019
ACS Sens. 2020, 5, 3306−3327

Table 1. continued

[a]CNT = carbon nanotubes, CPPy = 3-carboxylate polypyrrole, GO = graphene oxide, MEMS = microelectromechanical systems, NB = nanobelts, NG = nanogaps, NP = nanoparticles, NR = nanoribbons, NS = nanosheets, NT = nanotubes, NW = nanowires, PANI = polyaniline, PMMA = poly(methyl methacrylate), POSS = polyhedral oligomeric silsesquioxanes, PPy = polypyrrole, PTFE = polytetrafluoroethylene, PUA = polyurethane acrylate, rGO = reduced graphene oxide. [b]LoD = limit of detection.

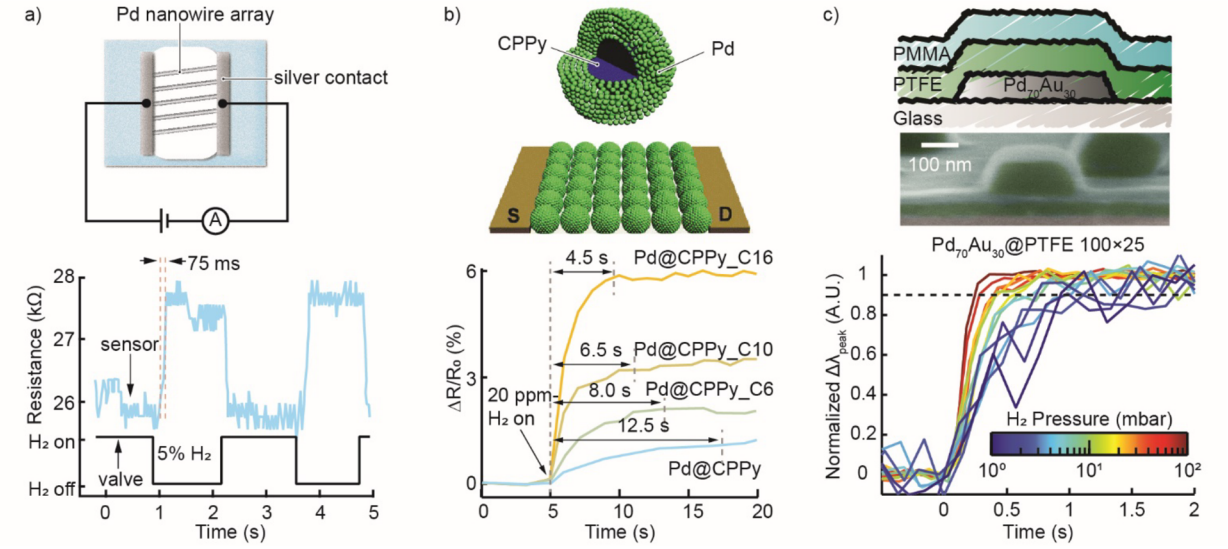

Figure 1. Fastest reported hydrogen sensors in the literature. (a) Pd mesowire array for resistive electrical readout—the first hydrogen sensor reported to achieve millisecond response time at 5 vol % H_2. Adapted with permission from ref 40. Copyright 2001 The American Association for the Advancement of Science. (b) Porous Pd nanoparticle-coated CPPy polymer hydrogen sensor using resistive electrical readout and exhibiting fast response even at ultralow 20 ppm of H_2 exposure. The numbers (C6−16) signify the length of the functionalized alkyl chain in the polymer. Adapted with permission from ref 24. Copyright 2015 Royal Society of Chemistry. (c) PMMA/PTFE-bilayer coated PdAu nanoparticle array hydrogen sensor using plasmonic optical readout—the first sensor to explicitly demonstrate <1 s response to 1 mbar H_2. Adapted with permission from ref 19. Copyright 2019 Nature Publishing Group.

deactivation by other molecular species is critical to consider when developing hydrogen sensors.

Cross-Sensitivity and Deactivation by Poisoning Gases and Humid Conditions. The presence of other molecular species than H_2 in the sensor environment may interfere with or completely disable the response of a hydrogen sensor via either cross-sensitivity or poisoning/deactivation. Cross-sensitivity here refers to how sensitive a sensor is toward unwanted stimulus by another species than the to-be-measured one and is thus related to selectivity. A perfectly selective sensor only responds to the species that is to be detected (H_2 in this case), while being completely inert toward other species. Practically, a sensor selectivity test is carried out by measuring sensor response upon exposure to pulses of different species. On the other hand, poisoning is sensor deactivation by one or multiple species that themselves do not induce a sensor signal but prevent H_2 detection due to, e.g., surface blockage. For certain systems, both phenomena can also occur at the same time. To this end, CO, NO_x, and sulfuric compounds are known to poison Pd-based hydrogen sensors.[19,58,82,83] In the US DoE targets (Scheme 1), cross-sensitivity is a main factor to determine the sensor accuracy while poisoning/deactivation is to sensor lifetime, accuracy, and response time.

In Table 2, we summarize studies from the same pool of fast hydrogen sensors surveyed above,[18] which have investigated the effect of interfering/poisoning species. It is clear that many studies performed selectivity tests, but only a few investigated poisoning/deactivation. Again, we see Pd as the main transducer material, due to its inherent excellent selectivity toward aliphatic/alcohol hydrocarbon species, such as CO, CO_2, C_2H_5OH, and CH_4. Furthermore, we note that testing sensor selectivity is particularly important for oxide-based sensors, because unlike Pd, they do not have inherent selectivity toward hydrogen gas. Therefore, oxide sensors usually employ a Pd coating/capping to improve the selectivity, as, for instance, shown for Pd-capped SnO_2 nanorods[84] and TiO_2 nanotubes.[85] Therefore, understanding the limiting factors of Pd−hydrogen interactions is equally important for this class of sensors.

With regard to sensor poisoning/deactivation, we found that this aspect is much less addressed than selectivity, despite its high relevance for real applications. For example, in the case of Pd-based sensors, species like CO, NO_x, sulfuric acid, and H_2O strongly interfere with hydrogen detection due to strong adsorption on the Pd surface, where they prevent H_2 dissociation and further absorption.[164−167] CO adsorption, for example, leads to (much) slower response times.[19,40,41,58,82,168] This, in turn, can also cause incorrect sensor readings that underestimate hydrogen concentration if sensor saturation is not achieved within the period of exposure.

A specific shortcoming of the handful of studies that do investigate the effects of sensor deactivation/poisoning is that, except for the work by Hayashi et al.,[96] none of the tests executed in the works presented in Table 2 follows the protocol suggested by ISO 26142, since all studies applied *premixed* H_2 and poisoning gases. The ISO 26142 protocol, however, suggests exposure to poisoning species *prior to* a H_2 pulse to test the poisoning effect, since this is closer to a scenario in a real setting.[169] Furthermore, although explicitly mentioned in the

https://dx.doi.org/10.1021/acssensors.0c02019
ACS Sens. 2020, 5, 3306−3327

Table 2. Selectivity and Poisoning Resistance Properties of Fast Hydrogen Sensors[18]

active materials[a]	background environment	tested gases	test type[b]	outcomes	ref
Pd@SnSe ultrathin film	N_2	C_2H_5OH, C_3H_6O, H_2O, NH_3, O_2	S	Excellent selectivity	86
SnO_2 thin film	Air	C_3H_8, CO, CO_2, NH_3	S	Excellent selectivity to C_3H_8, cross-sensitive to the rest	87
PdO@ZnO/PAN NF	N_2	CH_4, C_3H_8, CO	S	Excellent selectivity	88
WO_3 thin film	Air	CH_4, NO_2	S	Excellent selectivity	89
Pd/GO film	Air	H_2S, NH_3, NO_2	S	Fairly cross-sensitive	90
		30−70% RH	H	Decreased response amplitude	
PdAu@ZnO NP	Air	CH_3CHO, CH_4, C_2H_5OH, CO	S	Excellent selectivity to CH_4, fairly cross-sensitive to the rest	91
TiO_2@PPy	Air	CH_4, C_2H_5OH, C_3H_3, CO_2, NO_2	S	Cross-sensitive to CO_2, fairly cross-sensitive to C_3H_3, excellent selectivity to the rest	60
		5−95% RH	H	Decreased response amplitude	
MoS_2−Pt NP	Air	CO, NH_3, NO_2	S	Excellent selectivity	92
MoS_2 NS@ZnO thin film					93
Pd-WO_3 thin film	Air	CH_4, CO	S	Excellent selectivity	94
Heated Pd/SnO_2 NP			S	Excellent selectivity	95
			P	Excellent resistance	
Pd@SnO_2 NR	Air	CH_4, C_2H_2, CO	S	Excellent selectivity	84
		24−60% RH	H	Decreased response amplitude, decelerated response time	
$ZnFe_2O_4$−Pd@rGO	N_2	CO_2, NH_3	S	Excellent selectivity	39
		20−85% RH	H	Decreased response amplitude	
PdCuSi thin film	Air	$C_6H_{19}NSi_2$, H_2S, NO_2, SO_2	P	Decelerated response time	96
IRMOF-20	Air	CO_2, NO_2	S	Excellent selectivity	97
		40−90% RH	H	Maintained response amplitude	
Pt@SnO_2 NR	Air	CH_4, CO	S	Cross-sensitive	29
		22−84% RH	H	Decreased response amplitude, decelerated response time beyond 40% RH	
Heated Pd@Si NW	Air	CO	P	Excellent resistance	98
		8.5−43.4% RH	H	Excellent resistance	
WO_3−Pd_2Pd−Pt nanocomposite	Air	CH_4, CO_2, NH_3	S	Excellent selectivity	99
Pd NP@TiO_2 NT					85
Bi_2O_3 NR	Air	CH_3OH, C_2H_3OH, C_3H_8, CO, H−CHO, H_2S, NH_3, NO_2, SO_2	S	Excellent selectivity to CH_3OH, C_2H_3OH and NH_3, fairly cross-sensitive to the rest	100
Pd hollow NSh	N_2	CH_4, CO, CO_2	S	Excellent selectivity to CO_2, fairly cross-sensitive to the rest	101
PdAuCu NP	Air		P	Excellent resistance	58
PdNi thin film	N_2	H_2S, NH_3, SO_2	S	Fairly cross-sensitive to NH_3, excellent selectivity to the rest	61
PdCu NW	Air				70
Fe/TiO_2/ITO nanocomposite	Air	20−80% RH	H	Maintained response amplitude	102
PdAu NP @PTFE/PMMA	Air	CH_4, CO, CO_2, NO_2	P	Excellent resistance	19
Pd@MoO_3 NW	N_2	CH_3CH_2OH, CH_3OH, CO	S	Excellent selectivity	103
ZnO nanostructures	Air	C_2H_5OH, CO, CO_2, NO_2	S	Excellent selectivity to NO_2, cross sensitive to C_2H_5OH, fairly cross-sensitive to the rest	104
Nb_2O_5 NRo	Air	CH_4, NH_3	S	Excellent selectivity	105
La^{3+}@SnO_2 NF	Air	C_2H_5OH, C_4H_{10}, C_7H_8, CO	S	Fairly cross-sensitive to C_2H_5OH, excellent selectivity to the rest	106
Pd-WS_2/Si thin film	Air	C_2H_5OH, CO, H_2O, N_2, NH_3, O_2	S	Excellent selectivity	107
Pd@SnO_2 NRo	Air	C_2H_2, CO, CO_2	S	Excellent selectivity	108
MoO_3 NRo	Air	CH_3OH, C_2H_5OH, C_3H_6O, C_3H_8O, C_7H_8, CO	S	Excellent selectivity	52
MoO_3 NR/graphene					49
Pd−Pt@SiC thin film	Air	CO, H_2S, NH_3	S	Excellent selectivity	109
Pd NP@mesoporous WO_3	Air	C_2H_5OH, CO, H−CHO, NO_2	S	Excellent selectivity	110
Pd NP@GO	N_2	NO_2	S	Excellent selectivity	111
PdAu NR array	Air	20−60% RH	H	Maintained response amplitude	112
Pd thin film/AlN					113
rGO/ZnO/Pt nanocomposite	Air	CH_4, C_2H_4, C_4H_{10}, CO_2, NH_3, NO_2	S	Fairly cross-sensitive to CH_4 and C_2H_4, excellent selectivity to the rest	114
Pt NW	Air	CO, H_2O	S	Excellent selectivity	115
		15−50% RH	H	Decreased response amplitude	
Pt NP@WO_3	Air	35−87% RH	H	Maintained response amplitude	116

https://dx.doi.org/10.1021/acssensors.0c02019
ACS Sens. 2020, 5, 3306−3327

Table 2. continued

active materials[a]	background environment	tested gases	test type[b]	outcomes	ref
Thin film metallic glass/diamond/ZnO NR	Air	C_3H_6O, NH_3	S	Cross-sensitive	35
Mesoporous In_2O_3	Air	CH_2O, CH_2Cl_2, C_2H_5OH, $C_4H_8O_2$, C_8H_8, CO, NH_3, NO_3	S	Fairly cross-sensitive to $C_4H_8O_2$, cross-sensitive to CH_2O, excellent selectivity to the rest	117
Pt NP@WO_3/SiO_2	Air	17.8−71.5% RH	H	Maintained response amplitude, decelerated response time	118
Heated Pd NP@graphene	Air	50% RH	H	Excellent resistance	119
PdCuSi thin film	Air	CH_4, CO_2, He	S	Excellent selectivity	78
Pd strip@Si NM	Air	CO, H_2S, NH_3, NO_2	S	Fairly cross-sensitive to NO_2, excellent selectivity to the rest	120
		20−80% RH	H	Decreased response amplitude	
SnO_2 nanostructures	Air	CH_4, C_2H_5OH, CO	S	Cross-sensitive	121
NiO-Nb_2O_5 NP				Fairly cross-sensitive	122
MoO_3 NW				Fairly cross-sensitive to C_2H_5OH, excellent selectivity to the rest	123
CuO nanostructures				Cross-sensitive	124
Pd NP@Si nanomesh	Air	C_2H_5OH, C_7H_8, CO, H_2S, NO_2	S	Excellent selectivity	55
		30−80% RH	H	Decreased response amplitude, decelerated response time	
ZnO nanostructures	Air	CH_4	S	Fairly cross-sensitive	125
		33−84% RH	H	Maintained response amplitude	
Nb_2O_5 NRo	Air	C_2H_5OH, CO, NH_3	S	Cross-sensitive to NH_3, fairly cross-sensitive to the rest	126
Pd strip@3D structure	N_2	CH_4, CO_2, O_2	S	Excellent selectivity	127
Pd/ZnO NW	Air	CH_4, C_2H_5OH, C_3H_6O, CO	S	Excellent selectivity	33
La^{3+}@ZnO NR	Air	C_3H_6O, NH_3	S	Fairly cross-sensitive	48
C@ZnO NRo				Cross-sensitive	128
Pd-capped Mg thin film	Air	CO, CO_2, N_2, NO_2, O_2	S	Excellent selectivity	129−132
PdMg NW networks		40−80% RH	H	Decreased response amplitude	
PdPt NP@ZnO NRo					
PdPt ultrathin film					
Au-SnO_2 NP	Air	CO	S	Cross-sensitive	133
PPy NW			P	Decreased response amplitude	134
Nb_2O_5 NW			S	Fairly cross-sensitive	135
PtRu/Nafion			S	Cross-sensitive	136
Pd NP@graphene	Air	NH_3, NO_2	S	Fairly cross-sensitive	137
		40−80% RH	H	Maintained response amplitude, decelerated response time	
Sm-$CoFe_2O_4$ NP	Air	CH_4, C_2H_5OH, CO, CO_2, NO_2	S	Fairly cross-sensitive to C_2H_5OH and CO, excellent selectivity to the rest	138
		20−60% RH	H	Increased response amplitude	
Pd/V_2O_5 thin film	Air	CO, H_2S, NH_3	S	Excellent selectivity	139
		10−60% RH	H	Excellent resistance	
Si NW	Air	CH_3OH, CH_4, C_2H_5OH, C_3H_6O, C_3H_8O	S	Excellent selectivity to CH_4 and C_3H_6O, fairly cross-sensitive to the rest	140
Pd@Pt core@shell NP	Air	C_2H_2, C_3H_8, CO, CO_2, NO_2, O_2	S	Excellent selectivity	141
		33−92% RH	H	Decreased response amplitude, decelerated response time beyond 46% RH	
Pd thin film	Air	CH_3OH, C_2H_5OH, C_3H_6O, CO, NH_3	S	Fairly cross-sensitive NH_3, excellent selectivity to the rest	142
PdPt NP@Si NW	Air	40−80% RH	H	Decreased response amplitude	143
Cr_2O_3 NP@Nb_2O_5 nanostructures	Air	C_2H_5OH, H_2S, NH_3	S	Cross-sensitive	144
ZnCuO thin film	Air	CH_4, C_2H_5OH, CO	S	Excellent selectivity	145
Pd NP@TiO_2/PPy	Air	CH_3OH, CO_2, H_2S, NH_3	S	Excellent selectivity	146
Pd NP@PANI/rGO	Air	CH_3OH, CO_2, H_2S	S	Excellent selectivity	147
Pd NP@SnO_2 thin film	Air	C_3H_8, CO, NH_3	S	Excellent selectivity	148
Pd NP@TiO_2 NT	Air	5−20% RH	H	Decreased response amplitude	149
CNT	Air	CH_4, CO_2	S	Cross-sensitive	150
Pd NR	Air	CO_2	S	Excellent selectivity	151
Porous Pd NP@graphene	Air	C_2H_2, CO_x, N_2, NO_2, O_2	S	Excellent selectivity	152
SnO_2 NP@graphene	Air	CO, NO	S	Excellent selectivity	27
PdNi NP@graphene	Air	CO, CO_2, H_2O, NO_2, O_2	S	Excellent selectivity	153
Pt NP@TiO_2 NT	Air	CO, O_2	S	Excellent selectivity	154
		20−65% RH	H	Decreased response amplitude	

https://dx.doi.org/10.1021/acssensors.0c02019
ACS Sens. 2020, 5, 3306−3327

Table 2. continued

active materials[a]	background environment	tested gases	test type[b]	outcomes	ref
PdAu thin film	Air	CH_4, CO, O_2	P	Decreased response amplitude and decelerated response time to CO, excellent resistance to the rest	155
Pd NP@ZnO NR	Air	CO, CO_2, N_2, NO_2, O_2	S	Fairly cross-sensitive to NO_2, excellent selectivity to the rest	59
Cu-doped ZnO NRo	Air	CH_4, C_2H_5OH, C_3H_8, O_2	S	Excellent selectivity to CH_4 and C_3H_8, fairly cross-sensitive to the rest	156
CNT	Air	CH_4, C_2H_2, CO_2	S	Excellent selectivity	157
PdCuSi thin film	Air	CH_4, CO, CO_2	P	Decreased response amplitude and decelerated response time	158
Pd thin film	Air	Air, CH_4, CO, CO_2, H_2O, He, N_2	S	Excellent selectivity	159
Pt/YSZ/ITO thin film	Air	C_3H_6, CO, NH_3, NO, NO_2	S	Fairly cross-sensitive to C_3H_6, excellent selectivity to the rest	160
ZnO NRo	Air	CH_4, C_2H_5OH, C_3H_8, CO, O_2	S	Excellent selectivity	161
Pt doped-WO_3 thin film	Air	50−90% RH	H	Maintained response amplitude	162
Pd/TiO_2/polySi thin film	Air	C_2H_4, C_2H_5OH, NH_3	S	Excellent selectivity	163
Pd NP@Si NW	N_2	N_2O, NH_3	S	Excellent selectivity	76
Pd-coated rare earth thin film	Air	C_3H_8O, CO, H_2S	S	Excellent selectivity	31
Pd mesowire	Air	CO	P	Decelerated response time	40
	N_2	Ar, CH_4, CO, H_2O, O_2	S	Excellent selectivity	41

[a]CNT = carbon nanotubes, GO = graphene oxide, ITO = indium tin oxide, PAN = polyacrylonitrile, PANI = polyaniline, NF = nanofibers, NM = nanomembranes, NP = nanoparticles, NR = nanoribbons, NRo = nanorods, NS = nanosheets, NT = nanotubes, NSh = nanoshells, NW = nanowires, PANI = polyaniline, PPy = polypyrrole, rGO = reduced graphene oxide, YSZ = yttria-stabilized zirconia. [b]H = humidity test, P = poisoning test, S = selectivity test.

US DoE targets, the effect of H_2O vapor (humidity) is also rarely addressed. From the few studies that have investigated the impact of humidity (cf., Table 2), it is clear that it adversely affects the sensors by severely increasing the response time and decreasing response amplitude. However, some progress has been shown, for example, for Pd@Si nanowire[98] and PdAu alloy nanoribbon[112] sensors, which perform excellently at low humidity of 43% and 60% RH, respectively. The former owes its resistance to humid conditions to localized self-heating, while the latter employs an alloying effect to reduce H_2O adsorption on the Pd surface. However, none of the fast sensors have ever achieved acceptable humidity resistance in up to 95% RH, as required by the US DoE. Hence, investigating the impact of humidity and developing humidity-resistant solutions can be identified as a key challenge for future development in the area of hydrogen sensors.

Dynamic Range, Limit of Detection, and Power Consumption. When it comes to the dynamic range, the US DoE demands hydrogen sensors to be able to detect hydrogen concentration changes from 4 vol % (the lowest H_2 gas flammability limit in air) down to 0.1 vol % (Scheme 1). Overall, this requirement is essentially reached by all the surveyed hydrogen sensors, unlike response time and gas selectivity/poisoning discussed above. For instance, as shown in Table 1, *all* sensors exhibit detection limits well below the target of 0.1 vol %. As state-of-the-art, detection limits down to single-digit ppm, or even ppb, have been demonstrated.[19,24,27,32,33,170] These sensors are also capable of detecting hydrogen concentrations up to 4 vol %, although the response is usually not linear across this range of concentrations and rarely measured for both increasing and decreasing concentration. The former limits the concentration range across which the sensors exhibit high sensitivity (i.e., a significant change in sensor readout per H_2 concentration change), while the latter creates history-dependent sensor readout (i.e., hysteresis) and thus reduces accuracy within a certain pressure range. Both these aspects are very pronounced for pure Pd transducers, but strategies to alleviate these issues have been established, as we discuss in detail below.

Lastly, regarding sensor power consumption, the most stringent DoE target is 1 W (Scheme 1). A number of the fast Pd-based sensors listed in Table 1 exhibit power consumption as low as 1−100 nW[40,78,171] and none beyond 1 W. We note that all of them are electrical sensors. On the other hand, no works related to optical sensors report power consumption. However, examining available components (e.g., LEDs and photodiodes[172,173]) reveals that similar low power consumption as for electrical sensors can be expected.[174,175] Hence, reaching the US DoE power consumption standard seems feasible, irrespective of readout principle and transducer material.

Lifetime, Accuracy, Operation Temperature, and Absolute Operation Pressure. Operational lifetime is by definition the expected useful life of a sensor under operating conditions, while accuracy is the relationship between the sensor readout and the actual H_2 concentration.[17] Assessments of both aspects are normally first carried out at a prototype or product level.[176] In the surveyed fast sensors,[18] these two aspects have therefore not been addressed explicitly. Nevertheless, some efforts have been reported related to improving sensor lifetime and accuracy. For instance, to improve lifetime, deactivation-resistant sensors have been researched intensively, e.g., by alloying and polymer coatings.[19,58]

For the accuracy aspect, the main strategy has been the development of stable and deactivation-resistant transducer materials with low cross-sensitivity toward other analytes. To this end, sensor stability is usually examined by exposing the sensor to a large number of hydrogen cycles or by intermittent testing over a long period of time.[58,91,112] To the best of our knowledge, no specific recommendation for the minimal number of cycles exists, but we would recommend at least 50 cycles for such tests, ideally more.

In terms of operation temperature, for obvious reasons, fast sensors operating at high temperature (up to +85 °C, according

https://dx.doi.org/10.1021/acssensors.0c02019
ACS Sens. 2020, 5, 3306−3327

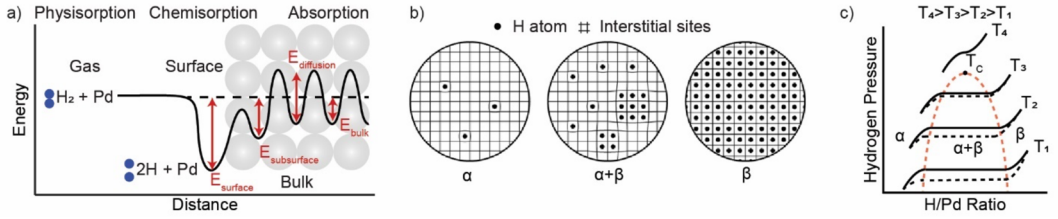

Figure 2. Palladium−hydrogen interaction. (a) Energy landscape encountered by a hydrogen molecule, H_2, upon interaction with a Pd surface. In the first step, the H_2 molecule dissociates on the Pd surface. In the next step, the formed hydrogen atoms, H, diffuse into the subsurface region and occupy subsurface interstitial lattice sites. Subsequently, H diffuses interstitially further into the bulk. (b) Schematic of the different stages of Pd hydride formation. In the low hydrogen pressure regime, H is highly diluted in a solid solution (α-phase), locally expanding the Pd host lattice. Increasing the equilibrium concentration of H in the lattice, as a consequence of a hydrogen pressure increase in the environment, eventually creates sizable attractive H−H interactions via strain fields and electronic interactions that promote the formation of hydride (β-phase) nuclei. The growth of the β-phase then continues until the entire Pd host is transformed, and it is accompanied by significant expansion of the lattice. (c) Schematic of pressure−composition isotherms of the Pd−hydrogen system and the corresponding phase diagram. The equilibrium plateau pressure, at which the α- and β-phases coexist, is temperature dependent and different for hydride formation and decomposition, due to hysteresis. The width of the plateau and the width of the hysteresis shrink for higher temperatures until they eventually vanish at the critical temperature, T_C.

to the Scheme 1) are much easier to find. However, we could not identify any works that explicitly examined the long-term stability of a sensor that operates at high temperature for a long period of time. This might not be an issue for metal-oxide based sensors, but for sensors employing, for example, high-aspect ratio Pd nanostructures, like nanowires,[20] nanostrips[127] and nanogaps[177] or polymer nanocomposites, such as PMMA/PTFE-coated Pd nanodisks[19] and Pd nanoparticles coated by CPPy,[24] high operation temperatures are likely to affect the shapes of the employed nanostructures and thus sensor performance. On the other end of the temperature scale, at low operational temperatures below RT, a small number of studies exist, reporting, for example, an amperometric proton-conducting clathrate hydrate based sensor (down to −20 °C),[178] a proton-conducting glass (−30 °C),[179] an optical sensor based on carbon nanotubes (−120 °C),[180] a Pt-doped WO_3 film (−50 °C), and a tapered fiber optic solution using a Pd thin-film as signal transducer (−196 °C).[181] All these works have in common very long response times on the order of minutes, with the exception of Bévenot et al., who utilized the local heating generated by the high-power laser diode used as light source in their Pd thin-film tapered fiber optic hydrogen sensor, which successfully enhanced the response time to 5 s for 4 vol % H_2 at −60 °C.[181]

Hydrogen sensor response variance at different absolute (atmospheric) pressures is another aspect that has not been scientifically addressed so far, since all studies we have surveyed have carried out their experiments at 1 atm (∼101 kPa). This is surprising since hydrogen sensors in, for example, automotive applications are very likely to be operated at varied altitudes.[7] To date, altitude or similar tests are first carried out at the prototype level and have a strong influence of the absolute atmospheric pressure on sensor response, even when the hydrogen partial pressure is kept constant.[176,182] We therefore advocate such tests taking place already at an earlier stage, when the active transducer materials are developed.

As an intermediate conclusion, it is clear that existing hydrogen sensors fulfill several of the US DoE performance targets, i.e., detection limit, selectivity, and power consumption. At the same time, a number of highly challenging targets remain unreached and relate to (i) response time, (ii) performance under poisoning/deactivation conditions, and (iii) in high humidity, operation at (iv) low/high temperature, and at (v) different absolute atmospheric pressure, where the last target (v) remains completely unaddressed. In other words, hydrogen sensor performance at *realistic* application conditions, rather than idealized laboratory environments, has rarely been addressed. In terms of active material, (nanostructured) Pd is most widely used due to its intrinsically high selectivity toward hydrogen combined with the potential for fast response (cf., Tables 1 and 2). Hence, to develop hydrogen sensors that are able to satisfy all of the stringent US DoE requirements and to alleviate the shortcomings of Pd as active material, one has to understand the fundamentals of the H−Pd interaction, as well as the opportunities offered by nanostructuring. Therefore, in the second part of this Perspective, we discuss these fundamentals and identify design rules for ultrafast, highly sensitive, poisoning- and humidity-resistant, and hysteresis-free hydrogen sensors.

HYDROGEN−PALLADIUM SYSTEM

Fundamentals of Pd−H Interactions and Their Implications for Hydrogen Detection. Pd enables an essentially barrierless hydrogen molecule (H_2) dissociation into chemisorbed hydrogen atoms (H) on its surface at ambient conditions (Figure 2a). Once these atoms have been formed, they rapidly saturate the surface and diffuse into interstitial lattice sites in the subsurface region, and finally into the bulk of the system at hand. Upon diffusing, the H atoms face an energy landscape (Figure 2a), which is characterized by energetically more favorable subsurface sites compared to bulk interstitials. Consequently, subsurface sites can be assumed occupied, regardless of the hydrogen concentration in the bulk. To this end, the extension of this subsurface hydrogen layer has been proposed to be between 0.3 and 1 nm.[183−186] Furthermore, it has been shown that the presence of hydrogen in the subsurface layer leads to the generation of lattice strain, which can influence the thermodynamics of the sorption process in nanoscale systems, such as nanoparticles.

Since the surface is the first and last contact of a hydrogen molecule upon interaction with Pd, it plays a key role in the sorption processes. Hence, any modification of the physical and chemical properties of the surface, such as impurities and strongly adsorbed molecules, or atomic rearrangement due to, e.g., refaceting or elemental surface segregation in an alloy, will to a certain degree affect the sorption processes by changing the overall energy landscape.[19,187−194] Furthermore, engineering the surface-to-volume ratio (SVR) of nanostructures provides a route to modify the sorption kinetics, where smaller structures

https://dx.doi.org/10.1021/acssensors.0c02019
ACS Sens. 2020, 5, 3306−3327

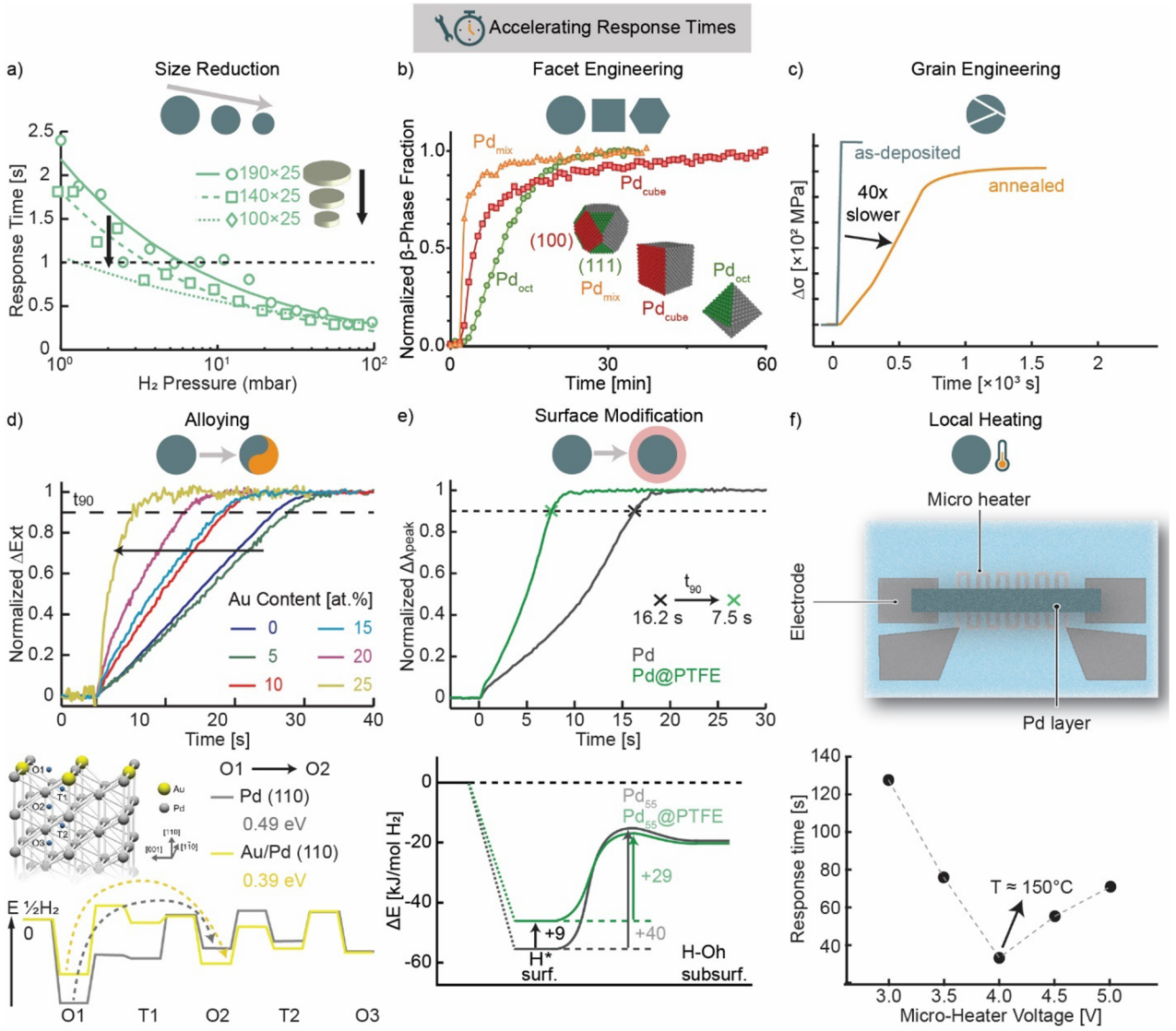

Figure 3. Different strategies to accelerate sensor response times. (a) Reducing the diameter of PTFE-coated PdAu alloy nanoparticles reduces response times across a wide range of applied H_2 pressure steps for this plasmonic optical sensor. Adapted with permission from ref 19 Copyright 2019 Nature Publishing Group. (b) Kinetics of hydrogenation of three types of colloidal Pd nanocrystals with different shapes and thus varying number of vertices. Pd_{mix} (24 vertices) responds fastest, followed by Pd_{cube} (8 vertices) and Pd_{oct} (6 vertices), highlighting the role of vertices as nucleation site for the β-phase. Adapted with permission from ref 193. Copyright 2019 Nature Publishing Group. (c) Kinetics of as-deposited and annealed Pd thin films upon hydrogenation. After annealing, the kinetics become 40 times slower due to significantly decreased density of grain boundaries in the film. Adapted with permission from ref 232. Copyright 2015 Elsevier. (d) Top: Temporal response of an optical hydrogen sensor comprising PdAu alloy nanoparticles with different Au contents. Increasing the Au content up to 25 at. % accelerates the kinetics. Adapted with permission from ref 231. Copyright 2015 American Chemical Society. Bottom: DFT-calculated hydrogen absorption energy landscape for neat Pd and a PdAu alloy. Note that for hydrogen diffusion from position O1 (surface) to O2 (subsurface), the PdAu alloy exhibits a lower activation barrier, explaining the faster absorption kinetics of the alloy observed in the experiments. O and T stand for octahedral and tetrahedral sites, respectively. The schematic shows the model used for calculation. Adapted with permission from ref 191. Copyright 2018 National Academy of Sciences of the United States of America. (e) Top: Temporal response of neat Pd nanoparticles to hydrogen with and without a 30 nm PTFE coating. Application of the coating reduces the response time by a factor 2. Bottom: DFT calculations reveal that the polymer coating reduces the activation barrier for H diffusion from the surface to a subsurface site and in this way accelerates sensor response. Adapted with permission from ref 19. Copyright 2019 Nature Publishing Group. (f) Top: Schematic of an electrical Pd film sensor that employs a resistive Pt heater for sensor operation at elevated temperature. Bottom: Response times of the sensor as a function of applied voltage showing the dramatic decrease of response time as temperature is increase up to 150 °C. At temperatures higher than 150 °C, the response time increase due to the counterbalance from hydrogen desorption. Adapted with permission from ref 233. Copyright 2012 Elsevier.

generally exhibit faster response.[19,23,195] However, for particles larger than 5−10 nm, this is not the consequence of an altered energy landscape due to, e.g., lattice strain,[196] but rather due to shorter diffusion lengths for H to reach the core of the structure.[197,198]

Once the surface is saturated with hydrogen, which for Pd occurs at very low pressures,[199] H species start occupying interstitial sites of the Pd host lattice to form a solid solution, which is known as α-phase (Figure 2b). In this regime, H is highly diluted and H−H interactions are very weak. Thus, the H/Pd ratio in the system increases proportionally to the square

https://dx.doi.org/10.1021/acssensors.0c02019
ACS Sens. 2020, 5, 3306−3327

root of pressure according to Sieverts' Law.[200] Upon increasing the hydrogen pressure, the H-concentration increases proportionally, such that attractive H−H interactions (both electronic and via lattice strain fields[199]) become appreciable. This eventually leads to the nucleation of the hydride (β-phase) at the two-phase equilibrium pressure (the "plateau"), where both α+β phases coexist as the system undergoes a first-order phase transformation (Figure 2b). Since the β-phase has a larger lattice constant than the Pd host (4.03 vs 3.89 Å),[201,202] this process is accommodated by significant lattice expansion, and the corresponding lattice strain is the origin of hysteresis between hydride formation and decomposition at constant temperature (Figure 2c).[183,184,203,204]

From a sensor perspective, the processes outlined above quite dramatically change both the electronic and optical properties of Pd and thus constitute the mechanism of hydrogen detection based on Pd, and explain Pd's intrinsically high hydrogen selectivity.[8,11] Specifically, for electrical hydrogen detection, the hydrogen absorption induces higher resistivity[21,205] or, in the case of discontinuous Pd nanostructures/films, expands their volume, which in turn forms new electrical contact points within the film/structures, resulting in reduced resistivity.[40,41] For optical hydrogen detection, the optical contrast generated due to hydrogen absorption into the host is measured (i) as a change in transmittance through a thin Pd film where it obeys the Beer−Lambert Law,[206,207] (ii) as a shift of the surface plasmon resonance (SPR) frequency of a thin Pd film,[77] or (iii) as a spectral shift of the localized surface plasmon resonance (LSPR) wavelength of Pd nanoparticles or nanostructures.[208,209] Also, indirect optical readout schemes based on inert plasmonic nanoantennas adjacent to a Pd nanostructure[184,210,211] or solutions based on nanostructured perfect absorbers[212,213] have been reported. They all have in common that the optical response is linearly correlated with the H/Pd ratio of the system.[207,209,214]

Another aspect of importance for hydrogen sensing with Pd is the two-phase coexistence plateau and the hysteresis between hydrogen absorption and desorption in this regime because it creates a number of problems. First, since the phase transformation to the hydride phase, and thus the generation of a large optical contrast or electric conductivity change, occurs in a very narrow pressure range, sensitivity on either side of the phase transformation is rather low. This is problematic, since at room temperature, hydride formation in Pd occurs at ∼20−30 mbar,[199] which means that sensitivity below (and above) this pressure will be low. Second, hysteresis renders the sensor signal to depend on the *history* of the hydrogen pressure, i.e., on which branch of the hysteresis loop the sensor is located at a specific point in time. This may create ambiguity in the sensor reading, which severely hampers its accuracy.

Effects of Nanostructuring. In the limit of (ultra) thin films, nanostructures and nanoparticles, the SVR increases and factors like subsurface or low-coordination sites start to play an increasingly important role.[193,198] A second aspect is the impact of lattice strain, induced either by surface tension effects in the sub-10 nm particle size range[195,215−219] or by the formation of a subsurface hydride layer in (larger) nanocrystals,[183,184,203] or along grain boundaries of polycrystalline nanoparticles.[220,221] These strain effects directly affect hysteresis and render it particle size dependent.[183,184,203,216−218,222−224] Similarly, in thin film systems, hysteresis can be suppressed by reducing the film thickness down to a few nanometers, due to clamping effects at the Pd−substrate interface.[225−228]

Another interesting effect observed in ultrasmall Pd nanoparticles, as well as in thin films with nanosized grains, is an *apparent* increased and decreased H solubility in the α- and β-phases, respectively.[218,229] Together, these two effects give rise to a narrowing of the two-phase coexistence plateau and have been explained by an increasing subsurface-to-bulk site ratio (nanoparticles)[223,224] and by the abundance of grain boundaries (thin films),[229] based on the fact that subsurface and grain boundary sites are likely to be fully occupied before the bulk, due to their favorable energetics.

As a final important trait of Pd nanostructures in general, and of Pd nanoparticles in particular, we note that the consequences of lattice expansion upon hydrogenation are not as severe as for bulk systems, where it is the main cause for embrittlement, cracking, and peeling when bound to a substrate, which in turn leads to rapid sensor aging and failure. Added to the fact that hydrogenation-induced defects are reversible during the reverse phase transformation in Pd nanoparticles,[230] nanostructured Pd hydrides promise potential for the improvement of sensor durability and thus sensor lifetime.

RATIONAL DESIGN OF NANOSTRUCTURED PD-BASED HYDROGEN SENSORS

Accelerating Response Times. In the quest to increase sensor speed, several different strategies have been tested and reported in the literature. The first one is based on the effect that increasing the SVR leads to faster sorption kinetics[198] (and thus response/recovery time) because (i) a larger surface area accelerates the hydrogen atom flux into the Pd and (ii) a smaller volume reduces diffusion path length to the core, as well as the total number of H atoms that need to be supplied to reach the new equilibrium state. This effect was first quantified in a fundamental study by Langhammer et al. for small (<5 nm) Pd nanoparticles.[195] In the context of sensors, this effect has been demonstrated on two examples using different nanostructures and sensing principles, namely, Pd nanowires with electrical readout[23] and PdAu alloy nanoparticles with optical readout (Figure 3a).[19,231] In both studies, clear proportionality between higher SVR and faster response time across all hydrogen concentrations (0.01−10 vol %) was found. By setting aside other factors influencing the kinetics, this finding suggests nanostructured Pd as the concept of choice for the design of ultrafast hydrogen sensors.

A second strategy to improve hydrogen sorption kinetics in nanostructured Pd is related to engineering its morphology, such as faceting and grain boundaries. For the former, a number of recent in situ investigations have shown that vertices of colloidal Pd nanocrystals act as hydride nucleation sites.[234−236] Building on this insight, a recent study by Johnson et al.[193] employed *single-crystalline* Pd nanocrystals with three different types of faceting, and thus different number of vertices, but with similar surface-to-bulk atom ratios achieved by adjusting size, i.e., octrahedral, cubic, and truncated cubic shape, which possess 6, 8, and 24 vertices, respectively (Figure 3b). By means of in situ XRD measurements, they showed that truncated cubic nanoparticles respond fastest when exposed to 5 vol % H_2, followed by the cubic and octahedral particles. Due to very similar surface-to-bulk-atom ratios of all particle types, they conclude proportionality between response time and number of vertices, highlighting the role of nanocrystal shape in Pd hydrogenation and thus for sensor applications of single crystalline Pd nanoparticles. For *polycrystalline* nanostructured Pd on the other hand, morphology engineering offers a handle to improve

https://dx.doi.org/10.1021/acssensors.0c02019
ACS Sens. 2020, 5, 3306−3327

response time since grain boundaries have been reported to act as rapid diffusion paths for hydrogen absorption due to the associated lower diffusion activation energy compared to interstitial diffusion within the crystal.[232,237−241] Specifically, to a stepwise 6 mbar H_2 exposure Delmelle et al. demonstrated 40 times slower response of an annealed (5 min at 350 °C) polycrystalline 150 nm Pd thin film compared to the as-prepared one (Figure 3c), due to significant recrystallization and corresponding reduction of total grain boundary length (40%) and defect density (30%), and average grain size increase from 20 to 49 nm.[232] However, we also note that other reports conclude an opposite effect of grain boundaries, i.e., that at very low H_2 concentrations grain boundaries act as traps for H, which was reported to decelerate kinetics.[240,241]

Beyond size reduction and morphology engineering, alloying of Pd provides yet another strategy to tackle the response time challenge, since characterization of the sorption kinetics of nanostructured Pd-alloy systems consistently reveals faster response than for the pure Pd counterparts, as first reported for PdNi alloy thin films[242] and PdAu alloy nanoparticles (Figure 3d).[231] Specifically for the latter system, systematic measurements revealed that increasing the Au concentration in the alloy results in a proportional acceleration of the hydrogen absorption process. These findings are confirmed in multiple studies using PdAu alloys in various forms,[19,243,244] as well as for other alloys, e.g., PdAg[245] and even the ternary system PdAuCu.[58] To this end, a recent DFT study by Namba et al. revealed that alloying Pd with Au lowers the energy barrier between surface and subsurface sites, which is responsible for the observed accelerated absorption (Figure 3d).[191] This is in good agreement with experimental works that investigated the apparent activation barriers for hydrogen sorption in PdAu[19] and PdCu nanoparticles.[58]

A fourth way to tailor the energy landscape for hydrogen sorption to accelerate response times is through interfacing the Pd surface with another material, such as a polymer or a metal−organic framework (MOF). This effect was first reported by Ngene et al. in 2014, who upon sputter-deposition of a 15 nm thin PTFE layer onto PdAu thin films found significantly faster hydrogen absorption.[246] XPS analysis revealed the formation of Pd−CF_x bonds at the PdAu/PTFE interface, which was proposed to create favorable adsorption sites for hydrogen. Further insights on the mechanism of the enhancement effect were later presented by Nugroho et al.,[19] who revealed by DFT calculations on the example of Pd and PdAu alloy nanoparticles that the presence of the PTFE layer, via bond formation, reduces the activation barrier for H to migrate from a surface site to a the subsurface site (Figure 3e). Interestingly, in the same study a similar acceleration effect was also observed for another and chemically different polymer, PMMA, although with slightly lower barrier reduction. These two examples hint at the genericity of the effect, which appears to be governed by bond formation between the Pd surface and the polymer, with specific barrier reduction depending on the polymer chemistry at hand. However, we also note that the polymer thickness has to be considered when designing such a coating. When it is too thick, the response time may deteriorate due to the increasing contribution of molecular H_2 diffusion through the polymer to the overall response.[247,248]

Similar to polymer coatings, also Pd coated with MOFs has been reported to feature superior hydrogen sorption kinetics. For example, Koo et al. found an improvement by a factor 20 when coating their Pd nanowires with a thin ZIF-8 layer and testing their sensor in air.[20] They put forward the filtering of O_2 by the MOF as the reason because O_2 is known to catalytically react with H_2 on the Pd surface to form water and thus "compete" with hydrogen sorption. However, we argue that this conclusion cannot explain similar acceleration effects observed when other Pd@MOFs were exposed to hydrogen in N_2 environment or even in pure H_2. For example, earlier work by Li et al. showed that a Pd nanocube@HKUST-1 system responds faster compared to its uncoated counterpart in *pure* H_2.[249] A followup DFT study by Nanba et al. then revealed that the MOF coating leads to an increased diffusion rate of hydrogen due to hydrogen adsorption destabilization induced by the Cu atom in the MOF.[250] They also propose a steric effect to take place, which creates a new hydrogen diffusion path through a Pd_5Cu octahedral site. Hence, their findings hint at a similar generic enhancement effect for MOFs as for polymer coatings. As a final comment, we note that coating with thin polymer or MOF layers provides an effective way to accelerate the Pd-based sensors' response not only through modification of absorption energy landscape but also via filtering of unwanted species that may poison or deactivate the sensor, as we discuss in detail below.[251]

To start the discussion of the last reported strategy for response time enhancement, we remind ourselves that hydrogen sorption in Pd is an activated process and therefore depends on temperature. Thus, heating a Pd-based sensor, for example, using an external heater, can accelerate its detection speed. This strategy is particularly important when the sensors are to be used in a low temperature environment. With a hydrogen absorption activation energy of 60−80 kJ/mol H_2 for pure Pd,[19,58,192,196] a mere 10 K temperature increase from RT will roughly double the sensor speed. This approach has been demonstrated by Yoon et al. by positioning the active Pd on a Pt microheater, which locally heats the active sensing area up to 150 °C (Figure 3f).[233] On the downside, however, heating will also reduce the absolute amount of hydrogen absorbed into the system, and therefore lower sensor signal amplitude for a specific hydrogen pressure change, meaning that also the limit of detection will be reduced.

From the above summary of different factors that affect Pd-based sensor response times, it is clear that the surface state of Pd is particularly important. Therefore, as the last point, we want to highlight here an aspect of high relevance when using colloidal Pd nanocrystals for hydrogen sensors, namely, that they inherently come with a surfactant (or similar) coating, applied during the synthesis in solution to both promote/block growth of specific surface facets and to prevent aggregation. To this end, in recent studies, the impact of the presence of the widely used ligands cetyltrimethylammonium bromide (CTAB), cetyltrimethylammonium chloride (CTAC), and tetraoctylammonium bromide (TOAB) has been investigated in detail. As the key conclusion, it was shown that their presence in the Pd surface increases response times significantly, as a consequence of an increased apparent activation barrier for hydrogen absorption.[192,194] At the same time, in line with the accelerating effect of a polymer coating discussed above, Stolás et al. showed that using the polymeric colloidal stabilizer poly(vinylpyrrolidone), PVP, instead accelerates the kinetics.[192] Similarly, post-synthesis removal of surfactants from the nanoparticles has been shown to amend the negative effects of their presence on the Pd nanoparticle surface.[252]

Suppressing Hysteresis. The inherent hysteresis between hydride formation and decomposition in pure Pd significantly

https://dx.doi.org/10.1021/acssensors.0c02019
ACS Sens. 2020, 5, 3306−3327

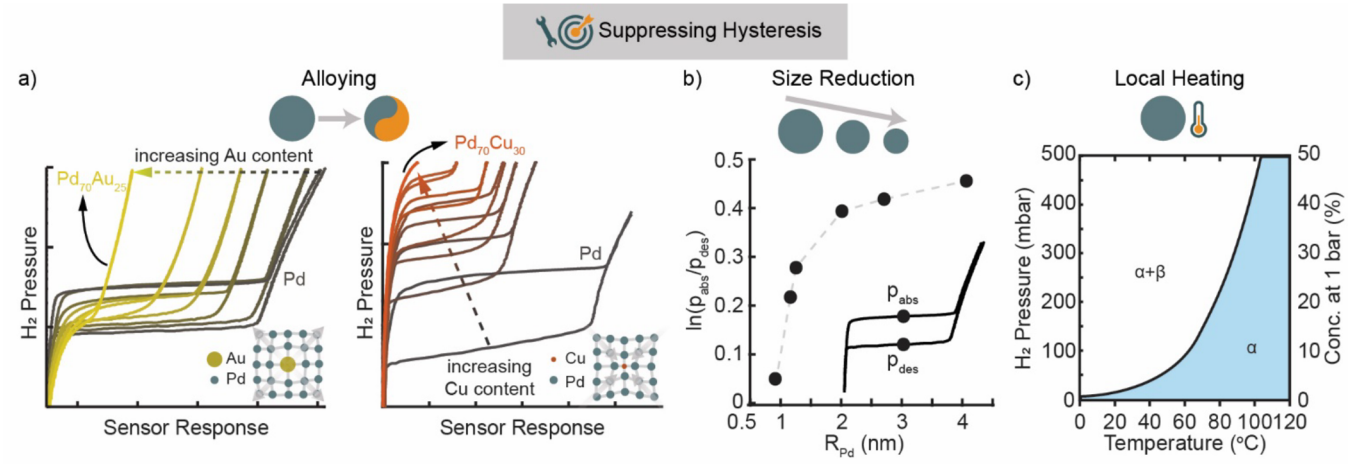

Figure 4. Strategies to suppress hysteresis in Pd. (a) Optical isotherms of PdAu (left) and PdCu (right) alloy nanoparticles measured at 30 °C. As the alloyant concentration increases, hysteresis shrinks and the α+β coexistence region narrows. Insets: Schematic of the lattice expansion and contraction induced by Au and Cu atoms, respectively. Adapted from refs 231 and 58. Copyright 2015 and 2019 American Chemical Society. (b) Hysteresis width, defined as $\ln(p_{abs}/p_{des})$, of small Pd nanoparticles in the sub-10 nm range, plotted as a function of their radius. Inset: Schematic showing the definition of p_{abs} and p_{des}. Adapted from ref 224. Copyright 2010 Elsevier. (c) Phase diagram of Pd hydride as a function of H_2 pressure/concentration and temperature. Hysteresis can be suppressed by operating the Pd-based sensor in a state of solid solution, denoted by the blue-shaded area. Adapted from ref 260. Copyright 2018 Elsevier.

reduces both dynamic range and accuracy of hydrogen sensors. Nevertheless, this challenge has not been addressed until rather recently by alloying Pd with other metals, including PdAu,[19,231,243,244,253] PdCu,[58] PdNi,[242] PdTa,[254] and ternary PdAuCu[58] and PdCuSi alloys.[255] Depending on the atomic radius of the alloyants, two types of pressure−composition isotherms exist. First, for alloyants with an atomic radius larger than Pd, e.g., Au, hysteresis shrinks symmetrically and disappears at room temperature (RT) at ca. 25 at % Au, since the critical temperature, T_C, at this concentration has been lowered to below RT (Figure 4a).[256] Mechanistically, this can be understood as the Au atoms, which occupy Pd lattice sites, slightly expanding the Pd host. Thereby, they reduce the strain-induced energy barrier created upon hydrogen sorption, and thus hysteresis.[256,257] To this end, Wadell et al. have shown that alloying Pd with 25 at % Au reduces sensor uncertainty to below 5% across the 1−1000 mbar H_2 pressure range,[231] which is on par with the corresponding performance target by the US DoE. Similarly, alloying with metals with smaller atomic radius than Pd, e.g., Cu[58] and Ni,[242] also suppresses hysteresis at ca. 25 at % alloyant concentration. However, due to a now slightly contracted Pd lattice that will increase the strain-induced energy barrier to form the hydride, hydride formation in this case occurs at higher pressures compared to neat Pd hydrogenated at the same temperature (Figure 4a).[258,259] From a sensing perspective, this leads to a lower sensitivity in the low hydrogen partial pressure regime.[209,255]

Another way to suppress hysteresis is through size reduction of the system to the regime below 10 nm. This was explicitly demonstrated by Langhammer et al., who systematically measured optical pressure−composition isotherms of Pd NPs of different size across the range between 1.8 and 8 nm and found that hysteresis vanishes for a size below ∼3 nm at 30 °C (Figure 4b).[215−217,224] Mechanistically, this can be understood through the so-called metal@hydride core@shell model. In this model, during the absorption (desorption) process, the hydride (metal) formation induces expansion (contraction) at the surface, while the metal (hydride) core shrinks. The volumetric difference between the two phases and the distortional deformation formed during the phase transformation lead to a mechanical stress at the interface of the two phases, which causes hysteresis. In sufficiently small nanoparticles, the corresponding strain energy is reduced and hysteresis therefore disappears.[224]

Similarly, also for a thin Pd film, hysteresis suppression can be achieved by reducing the thickness down to 5 nm as shown by Lee et al.[227] The suppression is due to the clamping effect by the support, which becomes more pronounced in an ultrathin Pd layer. This clamping restricts the Pd lattice such that it is energetically (too) costly to form the β-phase. Furthermore, the clamping effect depends on the support material,[226] and it can be intensified, for example, by a Ti buffer layer grown between the substrate and the Pd film.[225]

As the last strategy to reduce or completely avoid hysteresis in a sensor application, local heating of the active sensor area to above T_C can be applied to retain the system in the extended solid-solution state. For this purpose, Fisser et al. have provided a guideline for the corresponding hydrogen pressure and operational temperature required to retain a Pd thin film in the α-phase (Figure 4c).[260] For bulk Pd, T_C is 295 °C, while for small nanoparticles it decreases proportionally to their size.[203] As previously mentioned, however, limiting the sensing operation to the α-phase leads to a reduced limit of detection.

Protection against Poisoning Species and Humidity. Any surface at ambient conditions is covered by multilayers of molecular species present in air, including H_2O. Since the state of the surface is critical for any Pd-based hydrogen sensor, this is problematic. Among molecular species present in ambient air, CO chemisorbs strongly on Pd surfaces and thus effectively blocks it for H_2 dissociation (other species with similar effect are NO_x and SO_x[83,167]). This, in turn, significantly slows, or even completely prevents, hydrogen absorption into Pd. Therefore, finding ways to eliminate such poisoning effects is very important to ensure long-term reliable sensor operation. To this end, it is well-known that alloying Pd with Cu reduces the affinity of Pd surfaces to CO.[261−265] Hence, this concept has been successfully used in hydrogen separation membrane technology,[263,266] and since rather recently also in hydrogen sensing. Mak et al. employed $Pd_{70}Cu_{30}$ alloy thin films as optical

https://dx.doi.org/10.1021/acssensors.0c02019
ACS Sens. 2020, 5, 3306−3327

hydrogen sensor, however, with the main aim to reduce O_2 interference.[267] Then, Darmadi et al. presented a systematic study of optical PdCu alloy nanoparticle sensors with focus on CO poisoning, which showed that incorporating as little as 5 at % Cu to Pd effectively eliminates CO poisoning even at 5000 ppm CO in air (Figure 5a).[58] Interestingly, they also found that the added Cu works synergistically when combined with another alloyant, i.e., a ternary PdAuCu alloy resulted in a CO-resistant and hysteresis-free sensor. Unfortunately, however, with regard to other poisoning gases such as NO_2, this alloying strategy turned out to be insufficient.[58]

An alternative and potentially more broadly applicable strategy is the use of the molecular filtering properties of polymers or MOFs, when applied as coatings to a Pd-based active sensor surface. The efficiency of this approach is then directly dependent on the selectivity of the "filter" and the diffusivity of H_2 within it. If the latter is low, even if good protection is obtained, sensor response time will be dramatically increased. As an example for a polymer system, PMMA exhibits high H_2 permeability, while diffusivities of CO and NO_2 are very low.[269] Therefore, PMMA coatings have been used successfully to protect hydrogen sensors from these species.[19,82,168,247,248] For example, Nugroho et al. have demonstrated that a PMMA coating as thin as 30 nm is sufficient to enable the operation of a PdAu alloy optical hydrogen sensor in 30,000 ppm CO_2, 1000 ppm CO, and 100 ppm NO_2 mixed in synthetic air (Figure 5b). Furthermore, bulk-processed Pd@PMMA nanocomposite hydrogen sensors have been demonstrated to exhibit exceptional long-term stability at ambient conditions.[247] Finally, PMMA also possesses excellent selectivity toward O_2,[251] a trait that is shared with MOFs that have started to find application in hydrogen sensors as molecular filtering and protection layers, e.g., ZIF-8.[20,82,270]

Finally, we propose that employing the concept of a filtering coating may also hold the key to the development of highly humidity-tolerant hydrogen sensors and thereby tackle this so far widely unaddressed scientific challenge and resolve the corresponding DoE target. As one rare effort in this context, PTFE coatings have been utilized for humidity protection due to the inherently high hydrophobicity of fluorinated polymers,[268] and Mak et al. have utilized a 30 nm PTFE coating on an optical fiber sensor to demonstrate efficient hydrogen detection in oil.[267] As an alternative, alloying also may provide a means to increase the humidity resistance of Pd-based H_2 sensors, as demonstrated for the PdAu system, however, only up to 60% RH.[112] Last, locally heating the region where the active transducers are placed also provide a potentially effective strategy to reduce the detrimental impact of humidity, as demonstrated of the examples of heated Pd@Si nanowire[98] and Pd@graphene[119] hydrogen sensors.

FUTURE PERSPECTIVES

The recent acceleration in the large-scale global implementation of hydrogen energy technology has dramatically expedited the need for fast, selective, robust, and long-lived hydrogen safety sensors. In this respect, our assessment of state-of-the art hydrogen sensor technology has revealed a significant gap between currently available sensor performance and the performance targets set by stakeholders like the US DoE. This gap is, however, steadily closing, as a consequence of intense research activities in the field of hydrogen sensors during the last 15 years. For example, detection limits are now in the low ppm or even ppb range, and sensor response and recovery times have developed rapidly with the first reports of subsecond speed in the 1 mbar pressure regime, which is on par with the corresponding DoE target.

This development has predominantly been enabled by nanostructured Pd and Pd alloy transducer materials, which,

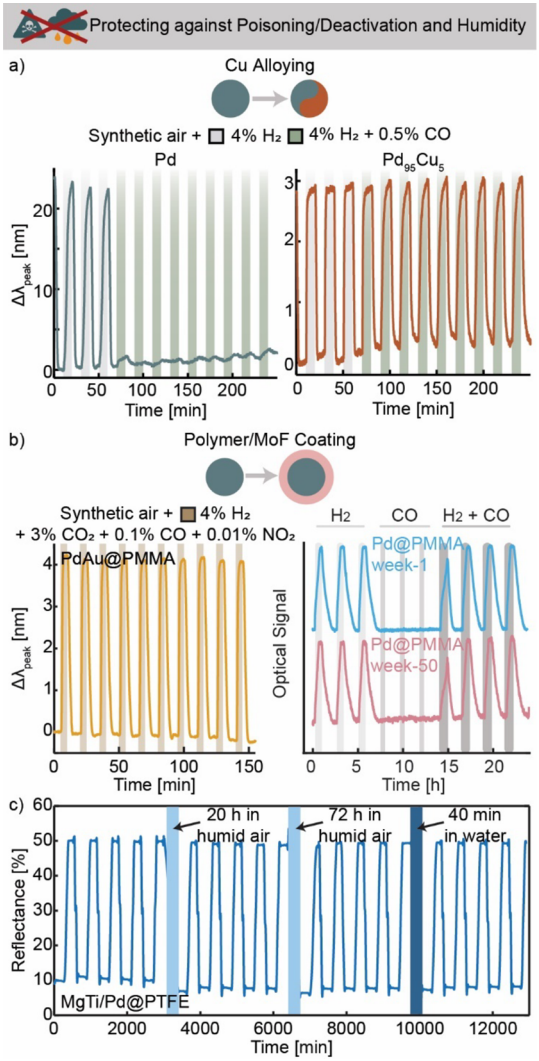

Figure 5. Strategies to protect Pd-based hydrogen sensors from poisoning/deactivation. (a) Time-dependent response of optical Pd (left) and $Pd_{95}Cu_5$ (right) nanoparticle hydrogen sensors to three 4% H_2 pulses, followed by 9 pulses of 4% H_2 + 0.5% CO in synthetic air. Alloying 5 at % Cu to Pd is sufficient to suppress the CO poisoning effect. Adapted from ref 58. Copyright 2019 American Chemical Society. (b) Left: Time-dependent response of optical PdAu nanoparticles@PMMA to pulses of 4% H_2 + 3% CO_2 + 0.1% CO + 0.01% NO_2 in synthetic air. PMMA provides efficient protection against all of the poisoning gases, resulting in a stable signal response over 10 cycles. Adapted with permission from ref 19. Copyright 2019 Nature Publishing Group. Right: Fresh and 50-weeks-aged Pd nanocube@PMMA 3D printed optical H_2 sensor response to three cycles of 10% H_2, three cycles of 0.5% CO, and four cycles of 10% H_2 + 0.5% CO, all in the synthetic air carrier gas. Adapted from ref 247. Copyright 2020 American Chemical Society. (c) Time-dependent reflectance of a MgTi/Pd@PTFE thin film hydrogen sensor to pulses of 5% H_2. Intermittently, the sensor was exposed to humid air and dipped in water, as marked. The PTFE layer provides significant protection as proven by unchanged response after each exposure to humid conditions. Adapted with permission from ref 268. Copyright 2012 The International Society for Optics and Photonics.

https://dx.doi.org/10.1021/acssensors.0c02019
ACS Sens. 2020, 5, 3306−3327

irrespective of the readout principle, offer intrinsically very high selectivity toward hydrogen thanks to the hydride formation process and rapid response due to short diffusion paths. It is therefore likely, and also our personal opinion, that clever engineering of Pd and Pd-alloy material properties at the nanoscale holds the key to even further push sensor detection limits and response times. At the same time, alternative material solutions are highly welcome since the foreseeable broadening of hydrogen sensor application conditions in the wake of the large-scale deployment of hydrogen energy technologies most likely requires increasingly tailored sensor solutions, which will be hard to provide on a single material platform alone. For example, hydride forming metals like Mg,[268,271] Ta,[272] V,[273] or Hf[272,274] may offer sensors with significantly wider dynamic range and unprecedented detection limits, however, at the cost of significantly longer response and recovery times, due to (orders of magnitude) slower hydrogen diffusion in these materials.

Other highly important metrics that have been much less addressed by the field are operation temperature, absolute-pressure range, sensor lifetime, and operation in poisoning/deactivating conditions and in high humidity. However, specifically for the last two points, interesting developments on the basis of polymeric or MOF coatings have been reported, where the molecular filtering properties of such layers have been demonstrated to prevent molecules larger than H_2 to reach the Pd surface, and thus hinder poisoning species from blocking the surface. Interestingly, if combined with nanoscale Pd transducers, the presence of such layers has also been reported to enhance response time, due to strong interactions between the metal surface and the coating. Furthermore, there are convincing indications that such hydrogen sorption kinetic enhancement effects are generic to both polymeric and MOF coatings, which fuels the hope that specific selection and optimization of coating materials in this respect may enable unprecedented response times. Here, however, the current lack of fundamental understanding of these effects hampers the identification of corresponding material design rules and calls for research efforts both by experiment and theory.

As a further key message to the community, we identify the almost complete lack of effort to design hydrogen sensors that can operate at high humidity levels up to 95% RH. This is critical in view of the fact that in the context of, for example, fuel cells, high humidity levels occur in the exhaust, and that hydrogen production sites at or close to, for example, offshore wind farms or offshore hydrogen pipelines will experience vast humidity fluctuations. Mechanistically, it is likely that the concept of coatings, as well as alloying, may hold the solution to this problem, but experimental demonstrations are widely lacking. Furthermore, the long-term stability of coatings or surface segregation effects in alloys are factors that need to be critically addressed, ideally already at the early active sensor material development stage, and not only at the sensor device prototype or product level, as commonly done today.

Finally, we want to highlight the need for more standardized hydrogen sensor characterization already at the research level to, for instance, enable more straightforward comparison of sensor performance, as well as to guarantee that sensor performance is measured at conditions relevant for targeted applications. This means the assessment of detection limits, operation temperatures, response and recovery times in (synthetic) air rather than in inert gas or even vacuum environments, and in the presence of trace molecular species found in the atmosphere, such as CO_2, NO_x, CO, SO_x and H_2O. It also means the assessment of response and recovery times over a wide(r) range of hydrogen concentrations since these performance parameters are strongly concentration dependent. We also advertise the adaptation of the ISO 26412 protocol for the assessment of poisoning/deactivation resistance of hydrogen sensors.

AUTHOR INFORMATION

Corresponding Authors

Iwan Darmadi − *Department of Physics, Chalmers University of Technology, 412 96 Göteborg, Sweden;* orcid.org/0000-0002-5921-9336; Email: darmadi@chalmers.se

Ferry Anggoro Ardy Nugroho − *DIFFER - Dutch Institute for Fundamental Energy Research, 5612 AJ Eindhoven, The Netherlands; Department of Physics and Astronomy, Vrije Universiteit Amsterdam, 1081 HV Amsterdam, The Netherlands;* orcid.org/0000-0001-5571-0454; Email: ferryanggoroardynugroho@yahoo.com

Christoph Langhammer − *Department of Physics, Chalmers University of Technology, 412 96 Göteborg, Sweden;* orcid.org/0000-0003-2180-1379; Email: clangham@chalmers.se

Complete contact information is available at: https://pubs.acs.org/10.1021/acssensors.0c02019

Author Contributions

The manuscript was written through contributions of all authors. All authors have given approval to the final version of the manuscript.

Notes

The authors declare the following competing financial interest(s): C.L. is co-founder of Insplorion AB that develops plasmonic hydrogen sensors.

ACKNOWLEDGMENTS

We acknowledge financial support from the Swedish Foundation for Strategic Research framework project RMA15-0052, from the Knut and Alice Wallenberg Foundation Project 2016.0210, and from Swedish Energy Agency project 49103-1. Parts of the TOC and figures use free-licensed resources from Freepik and Macrovector (www.freepik.com).

REFERENCES

(1) Crabtree, G. W.; Dresselhaus, M. S.; Buchanan, M. V. The Hydrogen Economy. *Phys. Today* **2004**, *57* (12), 39−44.

(2) *The European Green Deal: hydrogen is a priority area for a clean and circular economy*. https://www.fch.europa.eu/news/european-green-deal-hydrogen-priority-area-clean-and-circular-economy (accessed Aug 1, 2020).

(3) *A Hydrogen Strategy for a climate neutral Europe*. https://ec.europa.eu/commission/presscorner/detail/en/QANDA_20_1257 (accessed Aug 1, 2020).

(4) Randall, C. Norway: Explosion at hydrogen filling station https://www.electrive.com/2019/06/11/norway-explosion-at-fuel-cell-filling-station (accessed Aug 1, 2020).

(5) U.S. Department of Energy, Energy Efficiency and Renewable Energy (EERE), Fuel Cell Technologies Office. *Multi-Year Research, Development, and Demonstration Plan, 2011−2020. Section 3.7 Hydrogen Safety, Codes and Standards*; 2015.

(6) Palmisano, V.; Weidner, E.; Boon-Brett, L.; Bonato, C.; Harskamp, F.; Moretto, P.; Post, M. B.; Burgess, R.; Rivkin, C.; Buttner, W. J. Selectivity and Resistance to Poisons of Commercial Hydrogen Sensors. *Int. J. Hydrogen Energy* **2015**, *40* (35), 11740−11747.

(7) Boon-Brett, L.; Bousek, J.; Black, G.; Moretto, P.; Castello, P.; Hübert, T.; Banach, U. Identifying Performance Gaps in Hydrogen

Safety Sensor Technology for Automotive and Stationary Applications. *Int. J. Hydrogen Energy* **2010**, *35* (1), 373−384.
(8) Hübert, T.; Boon-Brett, L.; Palmisano, V.; Bader, M. A. Developments in Gas Sensor Technology for Hydrogen Safety. *Int. J. Hydrogen Energy* **2014**, *39*, 20474−20483.
(9) Hübert, T.; Boon-Brett, L.; Black, G.; Banach, U. Hydrogen Sensors - A Review. *Sens. Actuators, B* **2011**, *157*, 329−352.
(10) Penner, R. M. A Nose for Hydrogen Gas: Fast, Sensitive H2 Sensors Using Electrodeposited Nanomaterials. *Acc. Chem. Res.* **2017**, *50* (8), 1902−1910.
(11) Ndaya, C. C.; Javahiraly, N.; Brioude, A. Recent Advances in Palladium Nanoparticles-Based Hydrogen Sensors for Leak Detection. *Sensors* **2019**, *19* (20), 4478.
(12) Pham, T. K. N.; Brown, J. J. Hydrogen Sensors Using 2-Dimensional Materials: A Review. *ChemistrySelect* **2020**, *5* (24), 7277−7297.
(13) Sharma, B.; Sharma, A.; Kim, J. S. Recent Advances on H2 Sensor Technologies Based on MOX and FET Devices: A Review. *Sens. Actuators, B* **2018**, *262*, 758−770.
(14) Bannenberg, L. J.; Boelsma, C.; Asano, K.; Schreuders, H.; Dam, B. Metal Hydride Based Optical Hydrogen Sensors. *J. Phys. Soc. Jpn.* **2020**, *89* (5), No. 051003.
(15) Zhang, Y.; Peng, H.; Qian, X.; Zhang, Y.; An, G.; Zhao, Y. Recent Advancements in Optical Fiber Hydrogen Sensors. *Sens. Actuators, B* **2017**, *244*, 393−416.
(16) Noh, J.-S.; Lee, J. M.; Lee, W.; Noh, J.-S.; Lee, J. M.; Lee, W. Low-Dimensional Palladium Nanostructures for Fast and Reliable Hydrogen Gas Detection. *Sensors* **2011**, *11* (1), 825−851.
(17) Buttner, W.; Burgess, R. M.; Post, M.; Rivkin, C. *Summary and Findings from the NREL/DOE Hydrogen Sensor Workshop (June 8, 2011)*; Colorado, 2011.
(18) A search in Scopus as ″ TITLE-ABS-KEY(″*fast″ OR rapid OR quick) AND TITLE-ABS-KEY (hydrogen OR H2 PRE/1 sens* OR detect*) AND NOT TITLE(H2O2 OR peroxide) AND NOT TITLE(sulfide OR H2S) AND (LIMIT-TO (SRCTYPE,″j″)) AND (LIMIT-TO (DOCTYPE,″ar″)) AND (EXCLUDE (SUBJAREA,″EART″) OR EXCLUDE (SUBJAREA,″SOCI″)) AND (LIMIT-TO (LANGUAGE,″English″))″, accessed Sep 1 2020. We further refined the obtained list to remove unrelated works including review articles. The full list of articles we use in this Perspective can be dowloaded at https://tinyurl.com/Perspective-ACSSensors-Darmadi
(19) Nugroho, F. A. A.; Darmadi, I.; Cusinato, L.; Susarrey-Arce, A.; Schreuders, H.; Bannenberg, L. J.; da Silva Fanta, A. B.; Kadkhodazadeh, S.; Wagner, J. B.; Antosiewicz, T. J.; et al. Metal−Polymer Hybrid Nanomaterials for Plasmonic Ultrafast Hydrogen Detection. *Nat. Mater.* **2019**, *18*, 489−495.
(20) Koo, W. T.; Qiao, S.; Ogata, A. F.; Jha, G.; Jang, J. S.; Chen, V. T.; Kim, I. D.; Penner, R. M. Accelerating Palladium Nanowire H2 Sensors Using Engineered Nanofiltration. *ACS Nano* **2017**, *11* (9), 9276−9285.
(21) Li, X.; Liu, Y.; Hemminger, J. C.; Penner, R. M. Catalytically Activated Palladium@platinum Nanowires for Accelerated Hydrogen Gas Detection. *ACS Nano* **2015**, *9* (3), 3215−3225.
(22) Yang, F.; Taggart, D. K.; Penner, R. M. Fast, Sensitive Hydrogen Gas Detection Using Single Palladium Nanowires That Resist Fracture. *Nano Lett.* **2009**, *9* (5), 2177−2182.
(23) Yang, F.; Kung, S.-C.; Cheng, M.; Hemminger, J. C.; Penner, R. M. Smaller Is Faster and More Sensitive: The Effect of Wire Size on the Detection of Hydrogen by Single Palladium Nanowires. *ACS Nano* **2010**, *4* (9), 5233−5244.
(24) Lee, J. S.; Kim, S. G.; Cho, S.; Jang, J. Porous Palladium Coated Conducting Polymer Nanoparticles for Ultrasensitive Hydrogen Sensors. *Nanoscale* **2015**, *7* (48), 20665−20673.
(25) Kim, K. S.; Chung, G. S. Fast Response Hydrogen Sensors Based on Palladium and Platinum/Porous 3C-SiC Schottky Diodes. *Sens. Actuators, B* **2011**, *160* (1), 1232−1236.
(26) Kim, S. M.; Kim, H. J.; Jung, H. J.; Park, J.; Seok, T. J.; Choa, Y.; Park, T. J.; Lee, S. W. High-Performance, Transparent Thin Film Hydrogen Gas Sensor Using 2D Electron Gas at Interface of Oxide Thin Film Heterostructure Grown by Atomic Layer Deposition. *Adv. Funct. Mater.* **2018**, *29* (7), 1807760.
(27) Zhang, Z.; Zou, X.; Xu, L.; Liao, L.; Liu, W.; Ho, J.; Xiao, X.; Jiang, C.; Li, J. Hydrogen Gas Sensor Based on Metal Oxide Nanoparticles Decorated Graphene Transistor. *Nanoscale* **2015**, *7* (22), 10078−10084.
(28) Yang, P.; Li, X.; Huang, H.; Yang, S.; Zhang, X.; Hu, Y.; Wang, Z.; Gu, H. Hydrogen Sensing Kinetics of Laterally Aligned MoO3 Nanoribbon Arrays with Accelerated Response and Recovery Performances at Room Temperature. *Int. J. Hydrogen Energy* **2020**, *45* (43), 23841−23850.
(29) Chen, Z.; Hu, K.; Yang, P.; Fu, X.; Wang, Z.; Yang, S.; Xiong, J.; Zhang, X.; Hu, Y.; Gu, H. Hydrogen Sensors Based on Pt-Decorated SnO2 Nanorods with Fast and Sensitive Room-Temperature Sensing Performance. *J. Alloys Compd.* **2019**, *811*, 152086.
(30) Kathiravan, D.; Huang, B. R.; Saravanan, A. Multifunctional Sustainable Materials: The Role of Carbon Existing Protein in the Enhanced Gas and UV Sensing Performances of ZnO-Based Biofilms. *J. Mater. Chem. C* **2017**, *5* (21), 5239−5247.
(31) DiMeo, F.; Chen, I. S.; Chen, P.; Neuner, J.; Roerhl, A.; Welch, J. MEMS-Based Hydrogen Gas Sensors. *Sens. Actuators, B* **2006**, *117* (1), 10−16.
(32) Oh, J.; Lee, J. S.; Jang, J. Ruthenium Decorated Polypyrrole Nanoparticles for Highly Sensitive Hydrogen Gas Sensors Using Component Ratio and Protonation Control. *Polymers (Basel, Switz.)* **2020**, *12* (6), 1427.
(33) Lupan, O.; Postica, V.; Labat, F.; Ciofini, I.; Pauporté, T.; Adelung, R. Ultra-Sensitive and Selective Hydrogen Nanosensor with Fast Response at Room Temperature Based on a Single Pd/ZnO Nanowire. *Sens. Actuators, B* **2018**, *254*, 1259−1270.
(34) Xu, T.; Zach, M. P.; Xiao, Z. L.; Rosenmann, D.; Welp, U.; Kwok, W. K.; Crabtree, G. W. Self-Assembled Monolayer-Enhanced Hydrogen Sensing with Ultrathin Palladium Films. *Appl. Phys. Lett.* **2005**, *86* (20), 1−3.
(35) Huang, B. R.; Chu, J. P.; Saravanan, A.; Yenesew, M. M.; Bönninghoff, N.; Chang, C. H. High-Performance Sensor Based on Thin-Film Metallic Glass/Ultra-Nanocrystalline Diamond/ZnO Nanorod Heterostructures for Detection of Hydrogen Gas at Room Temperature. *Chem. - Eur. J.* **2019**, *25* (44), 10385−10393.
(36) Xiao, M.; Liang, S.; Han, J.; Zhong, D.; Liu, J.; Zhang, Z.; Peng, L. Batch Fabrication of Ultrasensitive Carbon Nanotube Hydrogen Sensors with Sub-Ppm Detection Limit. *ACS Sensors* **2018**, *3* (4), 749−756.
(37) Wang, J.; Singh, B.; Maeng, S.; Joh, H. I.; Kim, G. H. Assembly of Thermally Reduced Graphene Oxide Nanostructures by Alternating Current Dielectrophoresis as Hydrogen-Gas Sensors. *Appl. Phys. Lett.* **2013**, *103* (8), No. 083112.
(38) Chen, R.; Ruan, X.; Liu, W.; Stefanini, C. A Reliable and Fast Hydrogen Gas Leakage Detector Based on Irreversible Cracking of Decorated Palladium Nanolayer upon Aligned Polymer Fibers. *Int. J. Hydrogen Energy* **2015**, *40* (1), 746−751.
(39) Achary, L. S. K.; Maji, B.; Kumar, A.; Ghosh, S. P.; Kar, J. P.; Dash, P. Efficient Room Temperature Detection of H2 Gas by Novel ZnFe2O4−Pd Decorated RGO Nanocomposite. *Int. J. Hydrogen Energy* **2020**, *45* (7), 5073−5085.
(40) Favier, F.; Walter, E. C.; Zach, M. P.; Benter, T.; Penner, R. M. Hydrogen Sensors and Switches from Electrodeposited Palladium Mesowire Arrays. *Science (Washington, DC, U. S.)* **2001**, *293* (5538), 2227−2231.
(41) Walter, E. C.; Favier, F.; Penner, R. M. Palladium Mesowire Arrays for Fast Hydrogen Sensors and Hydrogen-Actuated Switches. *Anal. Chem.* **2002**, *74* (7), 1546−1553.
(42) Lee, J.; Noh, J. S.; Lee, S. H.; Song, B.; Jung, H.; Kim, W.; Lee, W. Cracked Palladium Films on an Elastomeric Substrate for Use as Hydrogen Sensors. *Int. J. Hydrogen Energy* **2012**, *37* (9), 7934−7939.
(43) Mattoni, G.; De Jong, B.; Manca, N.; Tomellini, M.; Caviglia, A. D. Single-Crystal Pt-Decorated WO3 Ultrathin Films: A Platform for Sub-Ppm Hydrogen Sensing at Room Temperature. *ACS Appl. Nano Mater.* **2018**, *1* (7), 3446−3452.

(44) Tsuji, T.; Mihara, R.; Saito, T.; Hagihara, S.; Oizumi, T.; Takeda, N.; Ohgi, T.; Yanagisawa, T.; Akao, S.; Nakaso, N.; et al. Highly Sensitive Ball Surface Acoustic Wave Hydrogen Sensor with Porous Pd-Alloy Film. *Mater. Trans.* **2014**, *55* (7), 1040−1044.
(45) Rumiche, F.; Wang, H. H.; Hu, W. S.; Indacochea, J. E.; Wang, M. L. Anodized Aluminum Oxide (AAO) Nanowell Sensors for Hydrogen Detection. *Sens. Actuators, B* **2008**, *134* (2), 869−877.
(46) Rumiche, F.; Wang, H. H.; Indacochea, J. E. Development of a Fast-Response/High-Sensitivity Double Wall Carbon Nanotube Nanostructured Hydrogen Sensor. *Sens. Actuators, B* **2012**, *163* (1), 97−106.
(47) Kyun, T. K.; Sang, J. S.; Sung, M. C. Hydrogen Gas Sensor Using Pd Nanowires Electro-Deposited into Anodized Alumina Template. *IEEE Sens. J.* **2006**, *6* (3), 509−513.
(48) Kathiravan, D.; Huang, B. R. Concurrent Enhancement in the H2 and UV Sensing Properties of ZnO Nanostructures through Discontinuous Lattice Coating of La3+: Via Partial p-n Junction Formation. *J. Mater. Chem. C* **2018**, *6* (9), 2387−2395.
(49) Yang, S.; Wang, Z.; Zou, Y.; Luo, X.; Pan, X.; Zhang, X.; Hu, Y.; Chen, K.; Huang, Z.; Wang, S.; et al. Remarkably Accelerated Room-Temperature Hydrogen Sensing of MoO3 Nanoribbon/Graphene Composites by Suppressing the Nanojunction Effects. *Sens. Actuators, B* **2017**, *248*, 160−168.
(50) Yatskiv, R.; Grym, J.; Zdansky, K.; Piksova, K. Semimetal Graphite/ZnO Schottky Diodes and Their Use for Hydrogen Sensing. *Carbon* **2012**, *50* (10), 3928−3933.
(51) Yu, S.; Welp, U.; Hua, L. Z.; Rydh, A.; Kwok, W. K.; Wang, H. H. Fabrication of Palladium Nanotubes and Their Application in Hydrogen Sensing. *Chem. Mater.* **2005**, *17* (13), 3445−3450.
(52) Yang, S.; Lei, G.; Lan, Z.; Xie, W.; Yang, B.; Xu, H.; Wang, Z.; Gu, H. Enhancement of the Room-Temperature Hydrogen Sensing Performance of MoO 3 Nanoribbons Annealed in a Reducing Gas. *Int. J. Hydrogen Energy* **2019**, *44* (14), 7725−7733.
(53) Tran, N. A.; Sang, C. H.; Pan, F. M.; Sheu, J. T. Controlled Functionalization of a Double-Junction N+/n-/N+ Polysilicon Nanobelt for Hydrogen Sensing Application. *Jpn. J. Appl. Phys.* **2016**, *55* (4), No. 04EM01.
(54) Zeng, X. Q.; Wang, Y. L.; Xiao, Z. L.; Latimer, M. L.; Xu, T.; Kwok, W. K. Hydrogen Responses of Ultrathin Pd Films and Nanowire Networks with a Ti Buffer Layer. *J. Mater. Sci.* **2012**, *47* (18), 6647−6651.
(55) Gao, M.; Cho, M.; Han, H.-J.; Jung, Y. S.; Park, I. Palladium-Decorated Silicon Nanomesh Fabricated by Nanosphere Lithography for High Performance, Room Temperature Hydrogen Sensing. *Small* **2018**, *14* (10), 1703691.
(56) Behzadi pour, G.; Fekri aval, L. Highly Sensitive Work Function Hydrogen Gas Sensor Based on PdNPs/SiO2/Si Structure at Room Temperature. *Results Phys.* **2017**, *7*, 1993−1999.
(57) Xie, B.; Zheng, M.; Liu, F.; Peng, X.; Wang, G.; Han, M. Fast Response Characteristics of Hydrogen Sensors Based on Pd Nanoparticle Films with Controlled Coverage. *J. Nanopart. Res.* **2013**, *15* (6), 1−8.
(58) Darmadi, I.; Nugroho, F. A. A.; Kadkhodazadeh, S.; Wagner, J. B.; Langhammer, C. Rationally Designed PdAuCu Ternary Alloy Nanoparticles for Intrinsically Deactivation-Resistant Ultrafast Plasmonic Hydrogen Sensing. *ACS Sensors* **2019**, *4* (5), 1424−1432.
(59) Rashid, T. R.; Phan, D. T.; Chung, G. S. A Flexible Hydrogen Sensor Based on Pd Nanoparticles Decorated ZnO Nanorods Grown on Polyimide Tape. *Sens. Actuators, B* **2013**, *185*, 777−784.
(60) Kumaresan, M.; Venkatachalam, M.; Saroja, M.; Gowthaman, P. Significant Enhancement in the Hydrogen-Sensing Performance of Polypyrrole/Titanium Oxide (PPy/TiO2) Hybrid Sensors by a Chemical Oxidation Polymerization Approach. *J. Mater. Sci.: Mater. Electron.* **2020**, *31* (11), 8183−8193.
(61) Wang, W.; Liu, X.; Mei, S.; Liu, M.; Lu, C.; Lu, M. Development of a High Stability Pd-Ni Alloy Thin-Film Coated SAW Device for Sensing Hydrogen. *Sensors* **2019**, *19* (16), 3560.
(62) Lee, J. M.; Park, J. E.; Kim, S.; Kim, S.; Lee, E.; Kim, S. J.; Lee, W. Ultra-Sensitive Hydrogen Gas Sensors Based on Pd-Decorated Tin Dioxide Nanostructures: Room Temperature Operating Sensors. *Int. J. Hydrogen Energy* **2010**, *35* (22), 12568−12573.
(63) Kong, J.; Chapline, M. G.; Dai, H. Functionalized Carbon Nanotubes for Molecular Hydrogen Sensors. *Adv. Mater.* **2001**, *13* (18), 1384−1386.
(64) Linke, S.; Dallmer, M.; Werner, R.; Moritz, W. Low Energy Hydrogen Sensor. *Int. J. Hydrogen Energy* **2012**, *37* (22), 17523−17528.
(65) Hsu, C. H.; Chang, C. C.; Tseng, C. M.; Chan, C. C.; Chao, W. H.; Wu, Y. R.; Wen, M. H.; Hsieh, Y. T.; Wang, Y. C.; Chen, C. L.; et al. An Ultra-Fast Response Gasochromic Device for Hydrogen Gas Detection. *Sens. Actuators, B* **2013**, *186*, 193−198.
(66) Mao, S.; Cui, S.; Yu, K.; Wen, Z.; Lu, G.; Chen, J. Ultrafast Hydrogen Sensing through Hybrids of Semiconducting Single-Walled Carbon Nanotubes and Tin Oxide Nanocrystals. *Nanoscale* **2012**, *4* (4), 1275−1279.
(67) Sirbuly, D. J.; Létant, S. E.; Ratto, T. V. Hydrogen Sensing with Subwavelength Optical Waveguides via Porous Silsesquioxane-Palladium Nanocomposites. *Adv. Mater.* **2008**, *20* (24), 4724−4727.
(68) Mao, S.; Zhou, H.; Wu, S.; Yang, J.; Li, Z.; Wei, X.; Wang, X.; Wang, Z.; Li, J. High Performance Hydrogen Sensor Based on Pd/TiO2 Composite Film. *Int. J. Hydrogen Energy* **2018**, *43* (50), 22727−22732.
(69) Xie, B.; Zhang, S.; Liu, F.; Peng, X.; Song, F.; Wang, G.; Han, M. Response Behavior of a Palladium Nanoparticle Array Based Hydrogen Sensor in Hydrogen-Nitrogen Mixture. *Sens. Actuators, A* **2012**, *181*, 20−24.
(70) Wang, W.; Liu, X.; Mei, S.; Jia, Y.; Liu, M.; Xue, X.; Yang, D. Development of a Pd/Cu Nanowires Coated SAW Hydrogen Gas Sensor with Fast Response and Recovery. *Sens. Actuators, B* **2019**, *287*, 157−164.
(71) Behzadi Pour, G.; Fekri Aval, L.; Esmaili, P. Performance of Gas Nanosensor in 1−4 per Cent Hydrogen Concentration. *Sens. Rev.* **2019**, *39* (4), 622−628.
(72) Sun, L.; Chen, M.; Peng, X.; Xie, B.; Han, M. The Effects of Ni Contents on Hydrogen Sensing Response of Closely Spaced Pd-Ni Alloy Nanoparticle Films. *Int. J. Hydrogen Energy* **2016**, *41* (2), 1341−1347.
(73) Chang, T.; Jung, H.; Jang, B.; Lee, J.; Noh, J. S.; Lee, W. Nanogaps Controlled by Liquid Nitrogen Freezing and the Effects on Hydrogen Gas Sensor Performance. *Sens. Actuators, A* **2013**, *192*, 140−144.
(74) Hussain, G.; Ge, M.; Zhao, C.; Silvester, D. S. Fast Responding Hydrogen Gas Sensors Using Platinum Nanoparticle Modified Microchannels and Ionic Liquids. *Anal. Chim. Acta* **2019**, *1072*, 35−45.
(75) Pan, Y. T.; Yin, X.; Kwok, K. S.; Yang, H. Higher-Order Nanostructures of Two-Dimensional Palladium Nanosheets for Fast Hydrogen Sensing. *Nano Lett.* **2014**, *14* (10), 5953−5959.
(76) Chen, Z. H.; Jie, J. S.; Luo, L. B.; Wang, H.; Lee, C. S.; Lee, S. T. Applications of Silicon Nanowires Functionalized with Palladium Nanoparticles in Hydrogen Sensors. *Nanotechnology* **2007**, *18* (34), 345502.
(77) Perrotton, C.; Westerwaal, R. J.; Javahiraly, N.; Slaman, M.; Schreuders, H.; Dam, B.; Meyrueis, P. A Reliable, Sensitive and Fast Optical Fiber Hydrogen Sensor Based on Surface Plasmon Resonance. *Opt. Express* **2013**, *21* (1), 382.
(78) Yamazaki, H.; Hayashi, Y.; Masunishi, K.; Ono, D.; Ikehashi, T. High Sensitivity MEMS Capacitive Hydrogen Sensor with Inverted T-Shaped Electrode and Ring-Shaped Palladium Alloy for Fast Response and Low Power Consumption. *J. Micromech. Microeng.* **2018**, *28* (9), No. 094001.
(79) Han, H.; Baik, S.; Xu, B.; Seo, J.; Lee, S.; Shin, S.; Lee, J.; Koo, J. H.; Mei, Y.; Pang, C.; et al. Bioinspired Geometry-Switchable Janus Nanofibers for Eye-Readable H2 Sensors. *Adv. Funct. Mater.* **2017**, *27* (29), 1701618.
(80) Jamnani, S. R.; Moghaddam, H. M.; Leonardi, S. G.; Neri, G. PANI/Sm2O3 Nanocomposite Sensor for Fast Hydrogen Detection at Room Temperature. *Synth. Met.* **2020**, *268*, 116493.

https://dx.doi.org/10.1021/acssensors.0c02019
ACS Sens. 2020, 5, 3306−3327

(81) Hübert, T. The H2Sense Hydrogen Sensor Database; https://netzwerke.bam.de/Netzwerke/Content/EN/Downloads/h2sense-database.pdf?__blob=publicationFile (accessed Mar 1, 2020).
(82) Kim, H.; Kim, W.; Cho, S.; Park, J.; Jung, G. Y. Molecular Sieve Based on a PMMA/ZIF-8 Bilayer for a CO-Tolerable H2 Sensor with Superior Sensing Performance. *ACS Appl. Mater. Interfaces* **2020**, *12* (25), 28616−28623.
(83) Burke, M. L.; Madix, R. J. Hydrogen on Pd(100)-S: The Effect of Sulfur on Precursor Mediated Adsorption and Desorption. *Surf. Sci.* **1990**, *237* (1−3), 1−19.
(84) Wang, F.; Hu, K.; Liu, H.; Zhao, Q.; Wang, K.; Zhang, Y. Low Temperature and Fast Response Hydrogen Gas Sensor with Pd Coated SnO2 Nanofiber Rods. *Int. J. Hydrogen Energy* **2020**, *45* (11), 7234−7242.
(85) Xiang, C.; She, Z.; Zou, Y.; Cheng, J.; Chu, H.; Qiu, S.; Zhang, H.; Sun, L.; Xu, F. A Room-Temperature Hydrogen Sensor Based on Pd Nanoparticles Doped TiO2 Nanotubes. *Ceram. Int.* **2014**, *40* (10), 16343−16348.
(86) Xu, H.; Liu, Y.; Liu, H.; Dong, S.; Wu, Y.; Wang, Z.; Wang, Y.; Wu, M.; Han, Z.; Hao, L. Pd-Decorated 2D SnSe Ultrathin Film on SiO2/Si for Room-Temperature Hydrogen Detection with Ultrahigh Response. *J. Alloys Compd.* **2021**, *851*, 156844.
(87) Zhang, H.; Li, Z.; Yi, J.; Zhang, H.; Zhang, Z. Potentiometric Hydrogen Sensing of Ordered SnO2 Thin Films. *Sens. Actuators, B* **2020**, *321*, 128505.
(88) Hwang, S.-H.; Kim, Y. K.; Jeong, S. M.; Choi, C.; Son, K. Y.; Lee, S.-K.; Lim, S. K. Wearable Colorimetric Sensing Fiber Based on Polyacrylonitrile with PdO@ZnO Hybrids for the Application of Detecting H_2 Leakage. *Text. Res. J.* **2020**, *90* (19−20), 2198−2211.
(89) Torabi Goodarzi, M.; Ranjbar, M. Atmospheric Flame Vapor Deposition of WO3 Thin Films for Hydrogen Detection with Enhanced Sensing Characteristics. *Ceram. Int.* **2020**, *46* (13), 21248−21255.
(90) Su, P. G.; Lin-Kuo, S. H2-Gas Sensing and Discriminating Actions of a Single-Yarn Sensor Based on a Pd/GO Multilayered Thin Film Using FFT. *Anal. Methods* **2020**, *12* (27), 3537−3544.
(91) Le, H. J.; Van Dao, D.; Yu, Y. T. Superfast and Efficient Hydrogen Gas Sensor Using PdAualloy@ZnO Core-Shell Nanoparticles. *J. Mater. Chem. A* **2020**, *8* (26), 12968−12974.
(92) Gottam, S. R.; Tsai, C. T.; Wang, L. W.; Wang, C. T.; Lin, C. C.; Chu, S. Y. Highly Sensitive Hydrogen Gas Sensor Based on a MoS2-Pt Nanoparticle Composite. *Appl. Surf. Sci.* **2020**, *506*, 144981.
(93) Gottam, S. R.; Tsai, C.-T.; Li, C.-Y.; Chu, S.-Y. Investigation of MoS2 Nanosheet-Coated ZnO Thin Films for Hydrogen Gas Sensing Applications and the Effect of Temperature on the Enhanced Sensor Response. *J. Electrochem. Soc.* **2020**, *167* (8), No. 087507.
(94) Han, Z.; Ren, J.; Zhou, J.; Zhang, S.; Zhang, Z.; Yang, L.; Yin, C. Multilayer Porous Pd-WO3 Composite Thin Films Prepared by Sol-Gel Process for Hydrogen Sensing. *Int. J. Hydrogen Energy* **2020**, *45* (11), 7223−7233.
(95) Sokovykh, E. V.; Oleksenko, L. P.; Maksymovych, N. P.; Matushko, I. P. Influence of Conditions of Pd/SnO2 Nanomaterial Formation on Properties of Hydrogen Sensors. *Nanoscale Res. Lett.* **2017**, *12* (1), 383.
(96) Hayashi, Y.; Yamazaki, H.; Masunishi, K.; Ikehashi, T.; Nakamura, N.; Kojima, A. Effects of Poisoning Gases on and Restoration of PdCuSi Metallic Glass in a Capacitive MEMS Hydrogen Sensor. *Int. J. Hydrogen Energy* **2020**, *45* (1), 1187−1194.
(97) Miliutina, E.; Guselnikova, O.; Chufistova, S.; Kolska, Z.; Elashnikov, R.; Burtsev, V.; Postnikov, P.; Svorcik, V.; Lyutakov, O. Fast and All-Optical Hydrogen Sensor Based on Gold-Coated Optical Fiber Functionalized with Metal-Organic Framework Layer. *ACS Sensors* **2019**, *4* (12), 3133−3140.
(98) Yun, J.; Ahn, J. H.; Moon, D. Il; Choi, Y. K.; Park, I. Joule-Heated and Suspended Silicon Nanowire Based Sensor for Low-Power and Stable Hydrogen Detection. *ACS Appl. Mater. Interfaces* **2019**, *11* (45), 42349−42357.
(99) Wang, G.; Qin, Y.; Dai, J.; Yang, S.; Ma, Y.; Zou, T.; Roths, J.; Yang, M. Performance-Enhanced Optical Fiber Hydrogen Sensors Based on WO3-Pd2Pt-Pt Composite Film with Controlled Optical Heating. *Opt. Fiber Technol.* **2019**, *52*, 101979.
(100) Shinde, P. V.; Ghule, B. G.; Shaikh, S. F.; Shinde, N. M.; Sangale, S. S.; Jadhav, V. V.; Yoon, S. Y.; Kim, K. H.; Mane, R. S. Microwave-Assisted Hierarchical Bismuth Oxide Worm-like Nanostructured Films as Room-Temperature Hydrogen Gas Sensors. *J. Alloys Compd.* **2019**, *802*, 244−251.
(101) Li, X.; Cao, T.; Zhang, X.; Sang, Y.; Yang, L.; Wang, T.; Li, Y.; Zhang, L.; Guo, L.; Fu, Y. Characterization and Optimization of the H2 Sensing Performance of Pd Hollow Shells. *Sens. Actuators, B* **2019**, *295*, 101−109.
(102) Monamary, A.; Vijayalakshmi, K.; Jereil, S. D. Fe Overlayered Hybrid TiO2/ITO Nanocomposite Sensor for Enhanced Hydrogen Sensing at Room Temperature by Novel Two Step Process. *Sens. Actuators, B* **2019**, *287*, 278−289.
(103) You, K.; Cao, F.; Wu, G.; Zhao, P.; Huang, H.; Wang, Z.; Hu, Y.; Gu, H.; Wang, J. Room-Temperature H 2 Gasochromic Behavior of Pd-Modified MoO 3 Nanowire Labels. *Mater. Chem. Phys.* **2019**, *227*, 111−116.
(104) Kumar, M.; Bhatt, V.; Kumar, A.; Yun, J. H. Nano Lily-Buds Garden like ZnO Nanostructures Based Gas Sensor for H 2 Detection. *Mater. Lett.* **2019**, *240*, 13−16.
(105) Pytlicek, Z.; Bendova, M.; Prasek, J.; Mozalev, A. On-Chip Sensor Solution for Hydrogen Gas Detection with the Anodic Niobium-Oxide Nanorod Arrays. *Sens. Actuators, B* **2019**, *284*, 723−735.
(106) Li, Z.; Yang, Q.; Wu, Y.; He, Y.; Chen, J.; Wang, J. La3+ Doped SnO 2 Nanofibers for Rapid and Selective H 2 Sensor with Long Range Linearity. *Int. J. Hydrogen Energy* **2019**, *44* (16), 8659−8668.
(107) Hao, L.; Liu, H.; Xu, H.; Dong, S.; Du, Y.; Wu, Y.; Zeng, H.; Zhu, J.; Liu, Y. Flexible Pd-WS2/Si Heterojunction Sensors for Highly Sensitive Detection of Hydrogen at Room Temperature. *Sens. Actuators, B* **2019**, *283*, 740−748.
(108) Kim, M. H.; Jang, B.; Kim, W.; Lee, W. Enhanced Hydrogen Sensing Properties of Pd-Coated SnO2 Nanorod Arrays in Nitrogen and Transformer Oil. *Sens. Actuators, B* **2019**, *283*, 890−896.
(109) Mourya, S.; Kumar, A.; Jaiswal, J.; Malik, G.; Kumar, B.; Chandra, R. Development of Pd-Pt Functionalized High Performance H2 Gas Sensor Based on Silicon Carbide Coated Porous Silicon for Extreme Environment Applications. *Sens. Actuators, B* **2019**, *283*, 373−383.
(110) Wu, C. H.; Zhu, Z.; Huang, S. Y.; Wu, R. J. Preparation of Palladium-Doped Mesoporous WO3 for Hydrogen Gas Sensors. *J. Alloys Compd.* **2019**, *776*, 965−973.
(111) Li, D.; Le, X.; Pang, J.; Peng, L.; Xu, Z.; Gao, C.; Xie, J. A SAW Hydrogen Sensor Based on Decoration of Graphene Oxide by Palladium Nanoparticles on AIN/Si Layered Structure. *J. Micromech. Microeng.* **2019**, *29* (4), No. 045007.
(112) Pak, Y.; Jeong, Y.; Alaal, N.; Kim, H.; Chae, J.; Min, J. W.; Devi, A. A. S.; Mitra, S.; Lee, D. H.; Kumaresan, Y.; et al. Highly Stable and Ultrafast Hydrogen Gas Sensor Based on 15 Nm Nanogaps Switching in a Palladium−Gold Nanoribbons Array. *Adv. Mater. Interfaces* **2019**, *6* (4), 1801442.
(113) Chen, D.; Wang, J. J.; Li, D. H.; Xu, Y. Hydrogen Sensor Based on Pd-Functionalized Film Bulk Acoustic Resonator. *Sens. Actuators, B* **2011**, *159* (1), 234−237.
(114) Drmosh, Q. A.; Yamani, Z. H.; Hendi, A. H.; Gondal, M. A.; Moqbel, R. A.; Saleh, T. A.; Khan, M. Y. A Novel Approach to Fabricating a Ternary RGO/ZnO/Pt System for High-Performance Hydrogen Sensor at Low Operating Temperatures. *Appl. Surf. Sci.* **2019**, *464*, 616−626.
(115) Cao, F.; Zhao, P.; Wang, Z.; Zhang, X.; Zheng, H.; Wang, J.; Zhou, D.; Hu, Y.; Gu, H. An Ultrasensitive and Ultraselective Hydrogen Sensor Based on Defect-Dominated Electron Scattering in Pt Nanowire Arrays. *Adv. Mater. Interfaces* **2019**, *6* (1), 1801304.
(116) Xu, B.; Chang, R.; Li, P.; Wang, D. N.; Zhao, C.-L.; Li, J. Q.; Yang, M.; Duan, L. Z. Reflective Optical Fiber Sensor Based on Light Polarization Modulation for Hydrogen Sensing. *J. Opt. Soc. Am. B* **2019**, *36* (12), 3471.

(117) Li, Z.; Yan, S.; Wu, Z.; Li, H.; Wang, J.; Shen, W.; Wang, Z.; Fu, Y. Q. Hydrogen Gas Sensor Based on Mesoporous In2O3 with Fast Response/Recovery and Ppb Level Detection Limit. *Int. J. Hydrogen Energy* **2018**, *43* (50), 22746−22755.
(118) Li, Y.; Shen, W.; Zhao, C.; Xu, B.; Wang, D.; Yang, M. Optical Hydrogen Sensor Based on PDMS-Formed Double-C Type Cavities with Embedded Pt-Loaded WO3/SiO2. *Sens. Actuators, B* **2018**, *276*, 23−30.
(119) Yokoyama, T.; Tanaka, T.; Shimokawa, Y.; Yamachi, R.; Saito, Y.; Uchida, K. Pd-Functionalized, Suspended Graphene Nanosheet for Fast, Low-Energy Multimolecular Sensors. *ACS Appl. Nano Mater.* **2018**, *1* (8), 3886−3894.
(120) Cho, M.; Yun, J.; Kwon, D.; Kim, K.; Park, I. High-Sensitivity and Low-Power Flexible Schottky Hydrogen Sensor Based on Silicon Nanomembrane. *ACS Appl. Mater. Interfaces* **2018**, *10* (15), 12870−12877.
(121) Liu, G.; Wang, Z.; Chen, Z.; Yang, S.; Fu, X.; Huang, R.; Li, X.; Xiong, J.; Hu, Y.; Gu, H. Remarkably Enhanced Room-Temperature Hydrogen Sensing of SnO2 Nanoflowers via Vacuum Annealing Treatment. *Sensors* **2018**, *18* (4), 949.
(122) Mirzaei, A.; Sun, G. J.; Lee, J. K.; Lee, C.; Choi, S.; Kim, H. W. Hydrogen Sensing Properties and Mechanism of NiO-Nb2O5 Composite Nanoparticle-Based Electrical Gas Sensors. *Ceram. Int.* **2017**, *43* (6), 5247−5254.
(123) Luo, X.; You, K.; Hu, Y.; Yang, S.; Pan, X.; Wang, Z.; Chen, W.; Gu, H. Rapid Hydrogen Sensing Response and Aging of A-MoO3 Nanowires Paper Sensor. *Int. J. Hydrogen Energy* **2017**, *42* (12), 8399−8405.
(124) Lupan, O.; Postica, V.; Ababii, N.; Hoppe, M.; Cretu, V.; Tiginyanu, I.; Sontea, V.; Pauporté, T.; Viana, B.; Adelung, R. Influence of CuO Nanostructures Morphology on Hydrogen Gas Sensing Performances. *Microelectron. Eng.* **2016**, *164*, 63−70.
(125) Lakshmanan, K.; Vijayakumari, A. M.; Basu, P. K. Reliable and Flow Independent Hydrogen Sensor Based on Microwave-Assisted ZnO Nanospheres: Improved Sensing Performance under UV Light at Room Temperature. *IEEE Sens. J.* **2018**, *18* (5), 1810−1819.
(126) Zou, Y.; He, J.; Hu, Y.; Huang, R.; Wang, Z.; Gu, Q. Room-Temperature Hydrogen Sensing Performance of Nb2O5 Nanorod Arrays. *RSC Adv.* **2018**, *8* (30), 16897−16901.
(127) He, J.; Villa, N. S.; Luo, Z.; An, S.; Shen, Q.; Tao, P.; Song, C.; Wu, J.; Deng, T.; Shang, W. Integrating Plasmonic Nanostructures with Natural Photonic Architectures in Pd-Modified: Morpho Butterfly Wings for Sensitive Hydrogen Gas Sensing. *RSC Adv.* **2018**, *8* (57), 32395−32400.
(128) Saravanan, A.; Huang, B. R.; Kathiravan, D.; Prasannan, A. Natural Biowaste-Cocoon-Derived Granular Activated Carbon-Coated ZnO Nanorods: A Simple Route to Synthesizing a Core-Shell Structure and Its Highly Enhanced UV and Hydrogen Sensing Properties. *ACS Appl. Mater. Interfaces* **2017**, *9* (45), 39771−39780.
(129) Hassan, K.; Chung, G.-S. Fast and Reversible Hydrogen Sensing Properties of Pd-Capped Mg Ultra-Thin Films Modified by Hydrophobic Alumina Substrates. *Sens. Actuators, B* **2017**, *242*, 450−460.
(130) Hassan, K.; Uddin, A. S. M. I.; Chung, G. S. Mesh of Ultrasmall Pd/Mg Bimetallic Nanowires as Fast Response Wearable Hydrogen Sensors Formed on Filtration Membrane. *Sens. Actuators, B* **2017**, *252*, 1035−1044.
(131) Hassan, K.; Chung, G. S. Catalytically Activated Quantum-Size Pt/Pd Bimetallic Core−Shell Nanoparticles Decorated on ZnO Nanorod Clusters for Accelerated Hydrogen Gas Detection. *Sens. Actuators, B* **2017**, *239*, 824−833.
(132) Hassan, K.; Iftekhar Uddin, A. S. M.; Chung, G. S. Fast-Response Hydrogen Sensors Based on Discrete Pt/Pd Bimetallic Ultra-Thin Films. *Sens. Actuators, B* **2016**, *234*, 435−445.
(133) Yin, X. T.; Tao, L. Fabrication and Gas Sensing Properties of Au-Loaded SnO2 Composite Nanoparticles for Low Concentration Hydrogen. *J. Alloys Compd.* **2017**, *727*, 254−259.
(134) Al-Mashat, L.; Debiemme-Chouvy, C.; Borensztajn, S.; Wlodarski, W. Electropolymerized Polypyrrole Nanowires for Hydrogen Gas Sensing. *J. Phys. Chem. C* **2012**, *116* (24), 13388−13394.
(135) Wang, Z.; Hu, Y.; Wang, W.; Zhang, X.; Wang, B.; Tian, H.; Wang, Y.; Guan, J.; Gu, H. Fast and Highly-Sensitive Hydrogen Sensing of Nb2O5 Nanowires at Room Temperature. *Int. J. Hydrogen Energy* **2012**, *37* (5), 4526−4532.
(136) Weng, Y. C.; Hung, K. C.; Wang, J. C.; Lee, Y. G.; Su, Y. F.; Lin, C. Y. Binary Platinum-Ruthenium/Nafion Electrodes for the Detection of Hydrogen. *Sens. Actuators, B* **2010**, *150* (1), 264−270.
(137) Alfano, B.; Polichetti, T.; Miglietta, M. L.; Massera, E.; Schiattarella, C.; Ricciardella, F.; Di Francia, G. Fully Eco-Friendly H2 Sensing Device Based on Pd-Decorated Graphene. *Sens. Actuators, B* **2017**, *239* (239), 1144−1152.
(138) Falsafi, F.; Hashemi, B.; Mirzaei, A.; Fazio, E.; Neri, F.; Donato, N.; Leonardi, S. G.; Neri, G. Sm-Doped Cobalt Ferrite Nanoparticles: A Novel Sensing Material for Conductometric Hydrogen Leak Sensor. *Ceram. Int.* **2017**, *43* (1), 1029−1037.
(139) Sanger, A.; Kumar, A.; Kumar, A.; Jaiswal, J.; Chandra, R. A Fast Response/Recovery of Hydrophobic Pd/V2O5 Thin Films for Hydrogen Gas Sensing. *Sens. Actuators, B* **2016**, *236*, 16−26.
(140) Qin, Y.; Wang, Y.; Liu, Y.; Zhang, X. KOH Post-Etching-Induced Rough Silicon Nanowire Array for H2 Gas Sensing Application. *Nanotechnology* **2016**, *27* (46), 465502.
(141) Uddin, A. S. M. I.; Yaqoob, U.; Hassan, K.; Chung, G. S. Effects of Pt Shell Thickness on Self-Assembly Monolayer Pd@Pt Core-Shell Nanocrystals Based Hydrogen Sensing. *Int. J. Hydrogen Energy* **2016**, *41* (34), 15399−15410.
(142) Hu, Y.; Lei, J.; Wang, Z.; Yang, S.; Luo, X.; Zhang, G.; Chen, W.; Gu, H. Rapid Response Hydrogen Sensor Based on Nanoporous Pd Thin Films. *Int. J. Hydrogen Energy* **2016**, *41* (25), 10986−10990.
(143) Hassan, K.; Uddin, A. S. M. I.; Chung, G. S. Hydrogen Sensing Properties of Pt/Pd Bimetal Decorated on Highly Hydrophobic Si Nanowires. *Int. J. Hydrogen Energy* **2016**, *41* (25), 10991−11001.
(144) Park, S.; Kheel, H.; Sun, G. J.; Kim, H. W.; Ko, T.; Lee, C. Room-Temperature Hydrogen Gas Sensing Properties of the Networked Cr2O3-Functionalized Nb2O5 Nanostructured Sensor. *Met. Mater. Int.* **2016**, *22* (4), 730−736.
(145) Lupan, O.; Cretu, V.; Postica, V.; Polonskyi, O.; Ababii, N.; Schütt, F.; Kaidas, V.; Faupel, F.; Adelung, R. Non-Planar Nanoscale p-p Heterojunctions Formation in ZnxCu1-XOy Nanocrystals by Mixed Phases for Enhanced Sensors. *Sens. Actuators, B* **2016**, *230*, 832−843.
(146) Zou, Y.; Wang, Q.; Jiang, D.; Xiang, C.; Chu, H.; Qiu, S.; Zhang, H.; Xu, F.; Sun, L.; Liu, S. Pd-Doped TiO2@polypyrrole Core-Shell Composites as Hydrogen-Sensing Materials. *Ceram. Int.* **2016**, *42* (7), 8257−8262.
(147) Zou, Y.; Wang, Q.; Xiang, C.; Tang, C.; Chu, H.; Qiu, S.; Yan, E.; Xu, F.; Sun, L. Doping Composite of Polyaniline and Reduced Graphene Oxide with Palladium Nanoparticles for Room-Temperature Hydrogen-Gas Sensing. *Int. J. Hydrogen Energy* **2016**, *41* (11), 5396−5404.
(148) Van Toan, N.; Viet Chien, N.; Van Duy, N.; Si Hong, H.; Nguyen, H.; Duc Hoa, N.; Van Hieu, N. Fabrication of Highly Sensitive and Selective H2 Gas Sensor Based on SnO2 Thin Film Sensitized with Microsized Pd Islands. *J. Hazard. Mater.* **2016**, *301*, 433−442.
(149) Moon, J.; Hedman, H. P.; Kemell, M.; Tuominen, A.; Punkkinen, R. Hydrogen Sensor of Pd-Decorated Tubular TiO2 Layer Prepared by Anodization with Patterned Electrodes on SiO2/Si Substrate. *Sens. Actuators, B* **2016**, *222*, 190−197.
(150) Shiraz, H. G.; Astaraei, F. R.; Fardindoost, S.; Hosseini, Z. S. Decorated CNT Based on Porous Silicon for Hydrogen Gas Sensing at Room Temperature. *RSC Adv.* **2016**, *6* (50), 44410−44414.
(151) Pak, Y.; Lim, N.; Kumaresan, Y.; Lee, R.; Kim, K.; Kim, T. H.; Kim, S.-M.; Kim, J. T.; Lee, H.; Ham, M.-H.; et al. Palladium Nanoribbon Array for Fast Hydrogen Gas Sensing with Ultrahigh Sensitivity. *Adv. Mater.* **2015**, *27* (43), 6945−6952.
(152) Phan, D. T.; Chung, G. S. A Novel Nanoporous Pd-Graphene Hybrid Synthesized by a Facile and Rapid Process for Hydrogen Detection. *Sens. Actuators, B* **2015**, *210*, 661−668.
(153) Phan, D. T.; Chung, G. S. Reliability of Hydrogen Sensing Based on Bimetallic Ni-Pd/Graphene Composites. *Int. J. Hydrogen Energy* **2014**, *39* (35), 20294−20304.

https://dx.doi.org/10.1021/acssensors.0c02019
ACS Sens. 2020, 5, 3306−3327

(154) Chen, K.; Xie, K.; Feng, X.; Tian, H.; Hu, R.; Li, Y.; Gu, H. Highly-Sensitive, Fast Hydrogen Sensing Employing Pt-Coated TiO2 Nanotube Arrays. *Funct. Mater. Lett.* **2014**, *7* (3), 1450021.
(155) Westerwaal, R. J.; Rooijmans, J. S. A.; Leclercq, L.; Gheorghe, D. G.; Radeva, T.; Mooij, L.; Mak, T.; Polak, L.; Slaman, M.; Dam, B.; et al. Nanostructured Pd−Au Based Fiber Optic Sensors for Probing Hydrogen Concentrations in Gas Mixtures. *Int. J. Hydrogen Energy* **2013**, *38* (10), 4201−4212.
(156) Chow, L.; Lupan, O.; Chai, G.; Khallaf, H.; Ono, L. K.; Roldan Cuenya, B.; Tiginyanu, I. M.; Ursaki, V. V.; Sontea, V.; Schulte, A. Synthesis and Characterization of Cu-Doped ZnO One-Dimensional Structures for Miniaturized Sensor Applications with Faster Response. *Sens. Actuators, A* **2013**, *189*, 399−408.
(157) Huang, B. R.; Lin, T. C. A Novel Technique to Fabricate Horizontally Aligned CNT Nanostructure Film for Hydrogen Gas Sensing. *Int. J. Hydrogen Energy* **2011**, *36* (24), 15919−15926.
(158) Kajita, S.; Yamaura, S. I.; Kimura, H.; Inoue, A. Hydrogen Sensing Ability of Pd-Based Amorphous Alloys. *Sens. Actuators, B* **2010**, *150* (1), 279−284.
(159) Patton, J. F.; Hunter, S. R.; Sepaniak, M. J.; Daskos, P. G.; Smith, D. B. Rapid Response Microsensor for Hydrogen Detection Using Nanostructured Palladium Films. *Sens. Actuators, A* **2010**, *163* (2), 464−470.
(160) Sekhar, P. K.; Brosha, E. L.; Mukundan, R.; Nelson, M. A.; Williamson, T. L.; Garzon, F. H. Development and Testing of a Miniaturized Hydrogen Safety Sensor Prototype. *Sens. Actuators, B* **2010**, *148* (2), 469−477.
(161) Lupan, O.; Chai, G.; Chow, L. Novel Hydrogen Gas Sensor Based on Single ZnO Nanorod. *Microelectron. Eng.* **2008**, *85* (11), 2220−2225.
(162) Caucheteur, C.; Debliquy, M.; Lahem, D.; Megret, P. Hybrid Fiber Gratings Coated with a Catalytic Sensitive Layer for Hydrogen Sensing in Air. *Opt. Express* **2008**, *16* (21), 16854.
(163) Chou, T. H.; Fang, Y. K.; Chiang, Y. T.; Lin, K. C.; Lin, C. I.; Kao, C.; Lin, H. Y. The Pd/TiO2/n-LTPS Thin-Film Schottky Diode on Glass Substrate for Hydrogen Sensing Applications. *IEEE Electron Device Lett.* **2008**, *29* (11), 1232−1235.
(164) Ogura, S.; Fukutani, K. Dynamic Blocking by CO of Hydrogen Transport across Pd 70 Au 30 (110) Surfaces. *J. Phys. Chem. C* **2017**, *121* (6), 3373−3380.
(165) Nyberg, C.; Tengstål, C. G. Adsorption and Reaction of Water, Oxygen, and Hydrogen on Pd(100): Identification of Adsorbed Hydroxyl and Implications for the Catalytic $H_2 - O_2$ Reaction. *J. Chem. Phys.* **1984**, *80* (7), 3463−3468.
(166) Ogura, S.; Okada, M.; Fukutani, K. Near-Surface Accumulation of Hydrogen and CO Blocking Effects on a Pd−Au Alloy. *J. Phys. Chem. C* **2013**, *117* (18), 9366−9371.
(167) Herron, J. A.; Tonelli, S.; Mavrikakis, M. Atomic and Molecular Adsorption on Pd(111). *Surf. Sci.* **2012**, *606* (21−22), 1670−1679.
(168) Hong, J.; Lee, S.; Seo, J.; Pyo, S.; Kim, J.; Lee, T. A Highly Sensitive Hydrogen Sensor with Gas Selectivity Using a PMMA Membrane-Coated Pd Nanoparticle/Single-Layer Graphene Hybrid. *ACS Appl. Mater. Interfaces* **2015**, *7* (6), 3554−3561.
(169) Buttner, W.; Rivkin, C.; Burgess, R. *Hydrogen Sensors*; 2015; pp 71−156. DOI: 10.1201/b19141-4.
(170) Koo, W.-T.; Kim, Y.; Kim, S.; Lee, S.-J. Hydrogen Sensors from Composites of Ultra- Small Bimetallic Nanoparticles and Porous Ion-Exchange Polymers. *Chem.* **2020**, *6*, 2746.
(171) Offermans, P.; Tong, H. D.; van Rijn, C. J. M.; Merken, P.; Brongersma, S. H.; Crego-Calama, M. Ultralow-Power Hydrogen Sensing with Single Palladium Nanowires. *Appl. Phys. Lett.* **2009**, *94* (22), 223110.
(172) Herkert, E.; Sterl, F.; Strohfeldt, N.; Walter, R.; Giessen, H. Low-Cost Hydrogen Sensor in the Ppm Range with Purely Optical Readout. *ACS Sensors* **2020**, *5* (4), 978−983.
(173) O'Toole, M.; Diamond, D. Absorbance Based Light Emitting Diode Optical Sensors and Sensing Devices. *Sensors* **2008**, *8* (4), 2453−2479.
(174) Gu, F.; Wu, G.; Zeng, H. Hybrid Photon-Plasmon Mach-Zehnder Interferometers for Highly Sensitive Hydrogen Sensing. *Nanoscale* **2015**, *7* (3), 924−929.
(175) Watanabe, T.; Okazaki, S.; Nakagawa, H.; Murata, K.; Fukuda, K. A Fiber-Optic Hydrogen Gas Sensor with Low Propagation Loss. *Sens. Actuators, B* **2010**, *145* (2), 781−787.
(176) Boon-Brett, L.; Bousek, J.; Castello, P.; Salyk, O.; Harskamp, F.; Aldea, L.; Tinaut, F. Reliability of Commercially Available Hydrogen Sensors for Detection of Hydrogen at Critical Concentrations: Part I − Testing Facility and Methodologies. *Int. J. Hydrogen Energy* **2008**, *33*, 7648−7657.
(177) Jang, B.; Cho, S.; Park, C.; Lee, H.; Song, M. J.; Lee, W. Palladium Nanogap-Based H2 Sensors on a Patterned Elastomeric Substrate Using Nanoimprint Lithography. *Sens. Actuators, B* **2015**, *221*, 593−598.
(178) Cha, J. H.; Lee, W.; Lee, H. Hydrogen Gas Sensor Based on Proton-Conducting Clathrate Hydrate. *Angew. Chem., Int. Ed.* **2009**, *48* (46), 8687−8690.
(179) Nogami, M.; Matsumura, M.; Daiko, Y. Hydrogen Sensor Prepared Using Fast Proton-Conducting Glass Films. *Sens. Actuators, B* **2006**, *120* (1), 266−269.
(180) Cusano, A.; Consales, M.; Cutolo, A.; Penza, M.; Aversa, P.; Giordano, M.; Guemes, A. Optical Probes Based on Optical Fibers and Single-Walled Carbon Nanotubes for Hydrogen Detection at Cryogenic Temperatures. *Appl. Phys. Lett.* **2006**, *89* (20), 201106.
(181) Bévenot, X.; Trouillet, A.; Veillas, C.; Gagnaire, H.; Clément, M. Hydrogen Leak Detection Using an Optical Fibre Sensor for Aerospace Applications. *Sens. Actuators, B* **2000**, *67* (1), 57−67.
(182) Ortiz Cebolla, R.; Weidner, E.; Buttner, W.; Bonato, C.; Hartmann, K.; Schmidt, K. Test Methodologies for Hydrogen Sensor Performance Assessment: Chamber vs. Flow-through Test Apparatus. *Int. J. Hydrogen Energy* **2018**, *43* (45), 21149−21160.
(183) Baldi, A.; Narayan, T. C.; Koh, A. L.; Dionne, J. A. In Situ Detection of Hydrogen-Induced Phase Transitions in Individual Palladium Nanocrystals. *Nat. Mater.* **2014**, *13* (12), 1143−1148.
(184) Syrenova, S.; Wadell, C.; Nugroho, F. A. A.; Gschneidtner, T. A.; Diaz Fernandez, Y. A.; Nalin, G.; Świtlik, D.; Westerlund, F.; Antosiewicz, T. J.; Zhdanov, V. P.; et al. Hydride Formation Thermodynamics and Hysteresis in Individual Pd Nanocrystals with Different Size and Shape. *Nat. Mater.* **2015**, *14* (12), 1236−1244.
(185) Gdowski, G. E.; Felter, T. E.; Stulen, R. H. Effect of Surface Temperature on the Sorption of Hydrogen by Pd(111). *Surf. Sci.* **1987**, *181* (3), L147−L155.
(186) Okuyama, H.; Siga, W.; Takagi, N.; Nishijima, M.; Aruga, T. Path and Mechanism of Hydrogen Absorption at Pd(100). *Surf. Sci.* **1998**, *401* (3), 344−354.
(187) *Hydrogen in Intermetallic Compunds II*, Schlapbach, L., Ed.; Topics in Applied Physics; Springer Berlin Heidelberg: Berlin, Heidelberg, 1992; Vol. *67*. DOI: 10.1007/3-540-54668-5.
(188) Christmann, K. Interaction of Hydrogen with Solid Surfaces. *Surf. Sci. Rep.* **1988**, *9* (1−3), 1−163.
(189) Cattania, M. G.; Penka, V.; Behm, R. J.; Christmann, K.; Ertl, G. Interaction of Hydrogen with a Palladium (110) Surface. *Surf. Sci.* **1983**, *126* (1−3), 382−391.
(190) Li, G.; Kobayashi, H.; Dekura, S.; Ikeda, R.; Kubota, Y.; Kato, K.; Takata, M.; Yamamoto, T.; Matsumura, S.; Kitagawa, H. Shape-Dependent Hydrogen-Storage Properties in Pd Nanocrystals: Which Does Hydrogen Prefer, Octahedron (111) or Cube (100)? *J. Am. Chem. Soc.* **2014**, *136* (29), 10222.
(191) Namba, K.; Ogura, S.; Ohno, S.; Di, W.; Kato, K.; Wilde, M.; Pletikosić, I.; Pervan, P.; Milun, M.; Fukutani, K. Acceleration of Hydrogen Absorption by Palladium through Surface Alloying with Gold. *Proc. Natl. Acad. Sci. U. S. A.* **2018**, *115* (31), 7896.
(192) Stolaś, A.; Darmadi, I.; Nugroho, F. A. A.; Moth-Poulsen, K.; Langhammer, C. Impact of Surfactants and Stabilizers on Palladium Nanoparticle−Hydrogen Interaction Kinetics: Implications for Hydrogen Sensors. *ACS Appl. Nano Mater.* **2020**, *3* (3), 2647−2653.
(193) Johnson, N. J. J.; Lam, B.; MacLeod, B. P.; Sherbo, R. S.; Moreno-Gonzalez, M.; Fork, D. K.; Berlinguette, C. P. Facets and

Vertices Regulate Hydrogen Uptake and Release in Palladium Nanocrystals. *Nat. Mater.* **2019**, *18* (5), 454−458.
(194) Johnson, N. J. J.; Lam, B.; Sherbo, R. S.; Fork, D. K.; Berlinguette, C. P. Ligands Affect Hydrogen Absorption and Desorption by Palladium Nanoparticles. *Chem. Mater.* **2019**, *31* (21), 8679−8684.
(195) Langhammer, C.; Zhdanov, V. P.; Zorić, I.; Kasemo, B. Size-Dependent Kinetics of Hydriding and Dehydriding of Pd Nanoparticles. *Phys. Rev. Lett.* **2010**, *104* (13), 135502.
(196) Grönbeck, H.; Zhdanov, V. P. Effect of Lattice Strain on Hydrogen Diffusion in Pd: A Density Functional Theory Study. *Phys. Rev. B: Condens. Matter Mater. Phys.* **2011**, *84* (5), No. 052301.
(197) Asakuma, Y.; Miyauchi, S.; Yamamoto, T.; Aoki, H.; Miura, T. Numerical Analysis of Absorbing and Desorbing Mechanism for the Metal Hydride by Homogenization Method. *Int. J. Hydrogen Energy* **2003**, *28* (5), 529−536.
(198) Bérubé, V.; Radtke, G.; Dresselhaus, M.; Chen, G. Size Effects on the Hydrogen Storage Properties of Nanostructured Metal Hydrides: A Review. *Int. J. Energy Res.* **2007**, *31* (6−7), 637−663.
(199) Manchester, F. D.; San-Martin, A.; Pitre, J. M. The H-Pd (Hydrogen-Palladium) System. *J. Phase Equilib.* **1994**, *15* (1), 62−83.
(200) Sieverts, A. Absorption of Gases by Metals. *Zeitschrift für Met.* **1929**, *21*, 37.
(201) Fukai, Y. *The Metal-Hydrogen System*; Springer-Verlag, 1993.
(202) Wicke, E.; Brodowsky, H.; Zuechner, H. Hydrogen in Palladium and Palladium Alloys. In *Hydrogen in Metals II*; Springer: Berlin Heidelberg, 1978; pp 73−155. DOI: 10.1007/3-540-08883-0_19.
(203) Griessen, R.; Strohfeldt, N.; Giessen, H. Thermodynamics of the Hybrid Interaction of Hydrogen with Palladium Nanoparticles. *Nat. Mater.* **2016**, *15* (3), 311−317.
(204) Schwarz, R. B.; Khachaturyan, A. G. Thermodynamics of Open Two-Phase Systems with Coherent Interfaces: Application to Metal−Hydrogen Systems. *Acta Mater.* **2006**, *54* (2), 313−323.
(205) Hughes, R. C.; Schubert, W. K. Thin Films of Pd/Ni Alloys for Detection of High Hydrogen Concentrations. *J. Appl. Phys.* **1992**, *71* (1), 542−544.
(206) Gremaud, R.; Broedersz, C. P.; Borsa, D. M.; Borgschulte, A.; Mauron, P.; Schreuders, H.; Rector, J. H.; Dam, B.; Griessen, R. Hydrogenography: An Optical Combinatorial Method To Find New Light-Weight Hydrogen-Storage Materials. *Adv. Mater.* **2007**, *19* (19), 2813−2817.
(207) Bannenberg, L. J.; Nugroho, F. A. A.; Schreuders, H.; Norder, B.; Trinh, T. T.; Steinke, N. J.; Van Well, A. A.; Langhammer, C.; Dam, B. Direct Comparison of PdAu Alloy Thin Films and Nanoparticles upon Hydrogen Exposure. *ACS Appl. Mater. Interfaces* **2019**, *11* (17), 15489−15497.
(208) Langhammer, C.; Zorić, I.; Kasemo, B.; Clemens, B. M. Hydrogen Storage in Pd Nanodisks Characterized with a Novel Nanoplasmonic Sensing Scheme. *Nano Lett.* **2007**, *7* (10), 3122−3127.
(209) Nugroho, F. A. A.; Darmadi, I.; Zhdanov, V. P.; Langhammer, C. Universal Scaling and Design Rules of Hydrogen-Induced Optical Properties in Pd and Pd-Alloy Nanoparticles. *ACS Nano* **2018**, *12* (10), 9903−9912.
(210) Liu, N.; Tang, M. L.; Hentschel, M.; Giessen, H.; Alivisatos, A. P. Nanoantenna-Enhanced Gas Sensing in a Single Tailored Nanofocus. *Nat. Mater.* **2011**, *10* (8), 631−636.
(211) Shegai, T.; Langhammer, C. Hydride Formation in Single Palladium and Magnesium Nanoparticles Studied by Nanoplasmonic Dark-Field Scattering Spectroscopy. *Adv. Mater.* **2011**, *23* (38), 4409−4414.
(212) Tittl, A.; Mai, P.; Taubert, R.; Dregely, D.; Liu, N.; Giessen, H. Palladium-Based Plasmonic Perfect Absorber in the Visible Wavelength Range and Its Application to Hydrogen Sensing. *Nano Lett.* **2011**, *11* (10), 4366−4369.
(213) ElKabbash, M.; Sreekanth, K. V.; Alapan, Y.; Kim, M.; Cole, J.; Fraiwan, A.; Letsou, T.; Li, Y.; Guo, C.; Sankaran, R. M.; et al. Hydrogen Sensing Using Thin-Film Perfect Light Absorber. *ACS Photonics* **2019**, *6* (8), 1889−1894.
(214) Palm, K. J.; Murray, J. B.; Narayan, T. C.; Munday, J. N. Dynamic Optical Properties of Metal Hydrides. *ACS Photonics* **2018**, *5* (11), 4677−4686.
(215) Wadell, C.; Pingel, T.; Olsson, E.; Zorić, I.; Zhdanov, V. P.; Langhammer, C. Thermodynamics of Hydride Formation and Decomposition in Supported Sub-10nm Pd Nanoparticles of Different Sizes. *Chem. Phys. Lett.* **2014**, *603*, 75−81.
(216) Yamauchi, M.; Ikeda, R.; Kitagawa, H.; Takata, M. Nanosize Effects on Hydrogen Storage in Palladium. *J. Phys. Chem. C* **2008**, *112* (9), 3294−3299.
(217) Narehood, D. G.; Kishore, S.; Goto, H.; Adair, J. H.; Nelson, J. A.; Gutiérrez, H. R.; Eklund, P. C. X-Ray Diffraction and H-Storage in Ultra-Small Palladium Particles. *Int. J. Hydrogen Energy* **2009**, *34* (2), 952−960.
(218) Sachs, C.; Pundt, A.; Kirchheim, R.; Winter, M.; Reetz, M. T.; Fritsch, D. Solubility of Hydrogen in Single-Sized Palladium Clusters. *Phys. Rev. B: Condens. Matter Mater. Phys.* **2001**, *64* (7), No. 075408.
(219) Yamauchi, M.; Kobayashi, H.; Kitagawa, H. Hydrogen Storage Mediated by Pd and Pt Nanoparticles. *ChemPhysChem* **2009**, *10* (15), 2566−2576.
(220) Alekseeva, S.; Fanta, A. B. da S.; Iandolo, B.; Antosiewicz, T. J.; Nugroho, F. A. A.; Wagner, J. B.; Burrows, A.; Zhdanov, V. P.; Langhammer, C. Grain Boundary Mediated Hydriding Phase Transformations in Individual Polycrystalline Metal Nanoparticles. *Nat. Commun.* **2017**, *8* (1), 1084.
(221) Mütschele, T.; Kirchheim, R. Hydrogen as a Probe for the Average Thickness of a Grain Boundary. *Scr. Metall.* **1987**, *21* (8), 1101−1104.
(222) Pundt, A.; Sachs, C.; Winter, M.; Reetz, M.; Fritsch, D.; Kirchheim, R. Hydrogen Sorption in Elastically Soft Stabilized Pd-Clusters. *J. Alloys Compd.* **1999**, *293*−*295*, 480−483.
(223) Pundt, A.; Suleiman, M.; Bähtz, C.; Reetz, M. T.; Kirchheim, R.; Jisrawi, N. M. Hydrogen and Pd-Clusters. *Mater. Sci. Eng., B* **2004**, *108* (1−2), 19−23.
(224) Langhammer, C.; Zhdanov, V. P.; Zorić, I.; Kasemo, B. Size-Dependent Hysteresis in the Formation and Decomposition of Hydride in Metal Nanoparticles. *Chem. Phys. Lett.* **2010**, *488* (1−3), 62−66.
(225) Kim, K. R.; Noh, J. S.; Lee, J. M.; Kim, Y. J.; Lee, W. Suppression of Phase Transitions in Pd Thin Films by Insertion of a Ti Buffer Layer. *J. Mater. Sci.* **2011**, *46* (6), 1597−1601.
(226) Othonos, A.; Kalli, K.; Tsai, D. P. Optically Thin Palladium Films on Silicon-Based Substrates and Nanostructure Formation: Effects of Hydrogen. *Appl. Surf. Sci.* **2000**, *161* (1), 54−60.
(227) Lee, E.; Lee, J. M.; Koo, J. H.; Lee, W.; Lee, T. Hysteresis Behavior of Electrical Resistance in Pd Thin Films during the Process of Absorption and Desorption of Hydrogen Gas. *Int. J. Hydrogen Energy* **2010**, *35* (13), 6984−6991.
(228) Baldi, A.; Gonzalez-Silveira, M.; Palmisano, V.; Dam, B.; Griessen, R. Destabilization of the Mg-H System through Elastic Constraints. *Phys. Rev. Lett.* **2009**, *102* (22), 226102.
(229) Li, Y.; Cheng, Y. T. Hydrogen Diffusion and Solubility in Palladium Thin Films. *Int. J. Hydrogen Energy* **1996**, *21* (4), 281−291.
(230) Ulvestad, A.; Yau, A. The Self-Healing of Defects Induced by the Hydriding Phase Transformation in Palladium Nanoparticles. *Nat. Commun.* **2017**, *8* (1), 1376.
(231) Wadell, C.; Nugroho, F. A. A.; Lidström, E.; Iandolo, B.; Wagner, J. B.; Langhammer, C. Hysteresis-Free Nanoplasmonic Pd-Au Alloy Hydrogen Sensors. *Nano Lett.* **2015**, *15* (5), 3563−3570.
(232) Delmelle, R.; Amin-Ahmadi, B.; Sinnaeve, M.; Idrissi, H.; Pardoen, T.; Schryvers, D.; Proost, J. Effect of Structural Defects on the Hydriding Kinetics of Nanocrystalline Pd Thin Films. *Int. J. Hydrogen Energy* **2015**, *40* (23), 7335−7347.
(233) Yoon, J. H.; Kim, B. J.; Kim, J. S. Design and Fabrication of Micro Hydrogen Gas Sensors Using Palladium Thin Film. *Mater. Chem. Phys.* **2012**, *133* (2−3), 987−991.
(234) Narayan, T. C.; Hayee, F.; Baldi, A.; Leen Koh, A.; Sinclair, R.; Dionne, J. A. Direct Visualization of Hydrogen Absorption Dynamics in Individual Palladium Nanoparticles. *Nat. Commun.* **2017**, *8*, 14020.

(235) Hayee, F.; Narayan, T. C.; Nadkarni, N.; Baldi, A.; Koh, A. L.; Bazant, M. Z.; Sinclair, R.; Dionne, J. A. In-Situ Visualization of Solute-Driven Phase Coexistence within Individual Nanorods. *Nat. Commun.* **2018**, *9* (1), 1 DOI: 10.1038/s41467-018-04021-1.
(236) Sytwu, K.; Hayee, F.; Narayan, T. C.; Koh, A. L.; Sinclair, R.; Dionne, J. A. Visualizing Facet-Dependent Hydrogenation Dynamics in Individual Palladium Nanoparticles. *Nano Lett.* **2018**, *18* (9), 5357.
(237) Iwaoka, H.; Arita, M.; Horita, Z. Hydrogen Diffusion in Ultrafine-Grained Palladium: Roles of Dislocations and Grain Boundaries. *Acta Mater.* **2016**, *107*, 168−177.
(238) Yau, A.; Harder, R. J.; Kanan, M. W.; Ulvestad, A. Imaging the Hydrogen Absorption Dynamics of Individual Grains in Polycrystalline Palladium Thin Films in 3D. *ACS Nano* **2017**, *11* (11), 10945−10954.
(239) Stuhr, U.; Striffler, T.; Wipf, H.; Natter, H.; Wettmann, B.; Janssen, S.; Hempelmann, R.; Hahn, H. An Investigation of Hydrogen Diffusion in Nanocrystalline Pd by Neutron Spectroscopy. *J. Alloys Compd.* **1997**, *253*−*254*, 393−396.
(240) Kirchheim, R. Hydrogen Solubility and Diffusivity in Defective and Amorphous Metals. *Prog. Mater. Sci.* **1988**, *32* (4), 261−325.
(241) Janßen, S.; Natter, H.; Hempelmann, R.; Striffler, T.; Stuhr, U.; Wipf, H.; Hahn, H.; Cook, J. C. Hydrogen Diffusion in Nanocrystalline PD by Means of Quasielastic Neutron Scattering. *Nanostruct. Mater.* **1997**, *9* (1−8), 579−582.
(242) Lee, E.; Lee, J. M.; Lee, E.; Noh, J.-S.; Joe, J. H.; Jung, B.; Lee, W. Hydrogen Gas Sensing Performance of Pd−Ni Alloy Thin Films. *Thin Solid Films* **2010**, *519* (2), 880−884.
(243) Nugroho, F. A. A.; Eklund, R.; Nilsson, S.; Langhammer, C. A Fiber-Optic Nanoplasmonic Hydrogen Sensor via Pattern-Transfer of Nanofabricated PdAu Alloy Nanostructures. *Nanoscale* **2018**, *10* (44), 20533−20539.
(244) Matuschek, M.; Singh, D. P.; Jeong, H. H.; Nesterov, M.; Weiss, T.; Fischer, P.; Neubrech, F.; Liu, N. Chiral Plasmonic Hydrogen Sensors. *Small* **2018**, *14* (7), 1702990.
(245) Jang, J.-S.; Qiao, S.; Choi, S.-J.; Jha, G.; Ogata, A. F.; Koo, W.-T.; Kim, D.-H.; Kim, I.-D.; Penner, R. M. Hollow Pd−Ag Composite Nanowires for Fast Responding and Transparent Hydrogen Sensors. *ACS Appl. Mater. Interfaces* **2017**, *9* (45), 39464−39474.
(246) Ngene, P.; Westerwaal, R. J.; Sachdeva, S.; Haije, W.; de Smet, L. C. P. M.; Dam, B. Polymer-Induced Surface Modifications of Pd-Based Thin Films Leading to Improved Kinetics in Hydrogen Sensing and Energy Storage Applications. *Angew. Chem., Int. Ed.* **2014**, *53* (45), 12081−12085.
(247) Darmadi, I.; Stolaś, A.; Östergren, I.; Berke, B.; Nugroho, F. A. A.; Minelli, M.; Lerch, S.; Tanyeli, I.; Lund, A.; Andersson, O.; et al. Bulk-Processed Pd Nanocube−Poly(Methyl Methacrylate) Nanocomposites as Plasmonic Plastics for Hydrogen Sensing. *ACS Appl. Nano Mater.* **2020**, *3* (8), 8438−8445.
(248) Chen, M.; Mao, P.; Qin, Y.; Wang, J.; Xie, B.; Wang, X.; Han, D.; Wang, G. H.; Song, F.; Han, M.; et al. Response Characteristics of Hydrogen Sensors Based on PMMA-Membrane-Coated Palladium Nanoparticle Films. *ACS Appl. Mater. Interfaces* **2017**, *9* (32), 27193−27201.
(249) Li, G.; Kobayashi, H.; Taylor, J. M.; Ikeda, R.; Kubota, Y.; Kato, K.; Takata, M.; Yamamoto, T.; Toh, S.; Matsumura, S.; et al. Hydrogen Storage in Pd Nanocrystals Covered with a Metal-Organic Framework. *Nat. Mater.* **2014**, *13* (8), 802−806.
(250) Nanba, Y.; Tsutsumi, T.; Ishimoto, T.; Koyama, M. Theoretical Study of the Hydrogen Absorption Mechanism into a Palladium Nanocube Coated with a Metal−Organic Framework. *J. Phys. Chem. C* **2017**, *121* (27), 14611−14617.
(251) Jeon, K.-J.; Moon, H. R.; Ruminski, A. M.; Jiang, B.; Kisielowski, C.; Bardhan, R.; Urban, J. J. Air-Stable Magnesium Nanocomposites Provide Rapid and High-Capacity Hydrogen Storage without Using Heavy-Metal Catalysts. *Nat. Mater.* **2011**, *10* (4), 286−290.
(252) Li, D.; Wang, C.; Tripkovic, D.; Sun, S.; Markovic, N. M.; Stamenkovic, V. R. Surfactant Removal for Colloidal Nanoparticles from Solution Synthesis: The Effect on Catalytic Performance. *ACS Catal.* **2012**, *2* (7), 1358−1362.
(253) Nugroho, F. A. A.; Iandolo, B.; Wagner, J. B.; Langhammer, C. Bottom-Up Nanofabrication of Supported Noble Metal Alloy Nanoparticle Arrays for Plasmonics. *ACS Nano* **2016**, *10* (2), 2871−2879.
(254) Westerwaal, R. J.; Duim, N.; Nieuwenhuijse, I.; Perrotton, C.; Dabirian, A.; Van Leeuwen, J. M.; Palmisano, V.; Dam, B. Thin Film Based Sensors for a Continuous Monitoring of Hydrogen Concentrations. *Sens. Actuators, B* **2012**, *165* (1), 88−96.
(255) Hayashi, Y.; Yamazaki, H.; Ono, D.; Masunishi, K.; Ikehashi, T. Investigation of PdCuSi Metallic Glass Film for Hysteresis-Free and Fast Response Capacitive MEMS Hydrogen Sensors. *Int. J. Hydrogen Energy* **2018**, *43* (19), 9438−9445.
(256) Luo, S.; Wang, D.; Flanagan, T. B. Thermodynamics of Hydrogen in Fcc Pd-Au Alloys. *J. Phys. Chem. B* **2010**, *114* (18), 6117−6125.
(257) Mamatkulov, M.; Zhdanov, V. P. Suppression of Hysteresis in Absorption of Hydrogen by a Pd-Au Alloy. *Phys. Rev. E: Stat. Phys., Plasmas, Fluids, Relat. Interdiscip. Top.* **2020**, *101* (4), 42130.
(258) Burch, R.; Buss, R. G. Absorption of Hydrogen by Palladium-Copper Alloys. Part 1. - Experimental Measurements. *J. Chem. Soc., Faraday Trans. 1* **1975**, *71*, 913−921.
(259) Burch, R.; Buss, R. G. Absorption of Hydrogen by Palladium-Copper Alloys. Part 2. - Theoretical Analysis. *J. Chem. Soc., Faraday Trans. 1* **1975**, *71*, 922−929.
(260) Fisser, M.; Badcock, R. A.; Teal, P. D.; Hunze, A. Optimizing the Sensitivity of Palladium Based Hydrogen Sensors. *Sens. Actuators, B* **2018**, *259*, 10−19.
(261) Rochefort, A.; Fournier, R. Quantum Chemical Study of CO and NO Bonding to Pd2, Cu2, and PdCu. *J. Phys. Chem.* **1996**, *100* (32), 13506−13513.
(262) Illas, F.; López, N.; Ricart, J. M.; Clotet, A.; Conesa, J. C.; Fernández-García, M. Interaction of CO and NO with PdCu(111) Surfaces. *J. Phys. Chem. B* **1998**, *102* (41), 8017−8023.
(263) O'Brien, C. P.; Lee, I. C. The Interaction of CO with PdCu Hydrogen Separation Membranes: An Operando Infrared Spectroscopy Study. *Catal. Today* **2019**, *336*, 216−222.
(264) Noordermeer, A.; Kok, G. A.; Nieuwenhuys, B. E. Comparison between the Adsorption Properties of Pd(111) and PdCu(111) Surfaces for Carbon Monoxide and Hydrogen. *Surf. Sci.* **1986**, *172* (2), 349−362.
(265) Debauge, Y.; Abon, M.; Bertolini, J. C.; Massardier, J.; Rochefort, A. Synergistic Alloying Behaviour of Pd50Cu50 Single Crystals upon Adsorption and Co-Adsorption of CO and NO. *Appl. Surf. Sci.* **1995**, *90* (1), 15−27.
(266) Zhang, K.; Way, J. D. Palladium-Copper Membranes for Hydrogen Separation. *Sep. Purif. Technol.* **2017**, *186*, 39−44.
(267) Mak, T.; Westerwaal, R. J.; Slaman, M.; Schreuders, H.; van Vugt, A. W.; Victoria, M.; Boelsma, C.; Dam, B. Optical Fiber Sensor for the Continuous Monitoring of Hydrogen in Oil. *Sens. Actuators, B* **2014**, *190*, 982−989.
(268) Slaman, M.; Westerwaal, R.; Schreuders, H.; Dam, B. Optical Hydrogen Sensors Based on Metal-Hydrides. *Proc. SPIE* **2012**, *8368*, 836805.
(269) Minelli, M.; Sarti, G. C. Elementary Prediction of Gas Permeability in Glassy Polymers. *J. Membr. Sci.* **2017**, *521*, 73−83.
(270) Weber, M.; Kim, J. H.; Lee, J. H.; Kim, J. Y.; Iatsunskyi, I.; Coy, E.; Drobek, M.; Julbe, A.; Bechelany, M.; Kim, S. S. High-Performance Nanowire Hydrogen Sensors by Exploiting the Synergistic Effect of Pd Nanoparticles and Metal-Organic Framework Membranes. *ACS Appl. Mater. Interfaces* **2018**, *10* (40), 34765−34773.
(271) Duan, X.; Griessen, R.; Wijngaarden, R. J.; Kamin, S.; Liu, N. Self-Recording and Manipulation of Fast Long-Range Hydrogen Diffusion in Quasifree Magnesium. *Phys. Rev. Mater.* **2018**, *2* (8), No. 085802.
(272) Bannenberg, L. J.; Boelsma, C.; Schreuders, H.; Francke, S.; Steinke, N. J.; van Well, A. A.; Dam, B. Optical Hydrogen Sensing beyond Palladium: Hafnium and Tantalum as Effective Sensing Materials. *Sens. Actuators, B* **2019**, *283*, 538−548.

(273) Orimo, S.; Günter Majer, F. K. Hydrogen in Nanostructured Vanadium-Hydrogen Systems. *Phys. Rev. B: Condens. Matter Mater. Phys.* **2001**, *63* (9), 943071−9430710.
(274) Boelsma, C.; Bannenberg, L. J.; van Setten, M. J.; Steinke, N.-J.; van Well, A. A.; Dam, B. Hafnium—an Optical Hydrogen Sensor Spanning Six Orders in Pressure. *Nat. Commun.* **2017**, *8*, 15718.

https://dx.doi.org/10.1021/acssensors.0c02019
ACS Sens. 2020, 5, 3306−3327